POLITECNICO DI TORINO
Repository ISTITUZIONALE

Mechanical Characterization and Constitutive Modelling of Commercial Biopolymers and Their Blends for Biomedical Applications

Original
Mechanical Characterization and Constitutive Modelling of Commercial Biopolymers and Their Blends for Biomedical Applications / Burgio, V., Di Giacinti, M., Rodriguez Reinoso, M., Tuveri, V., Antonaci, P., Surace, C.. - In: JOURNAL OF THE MECHANICAL BEHAVIOR OF BIOMEDICAL MATERIALS. - ISSN 1751-6161. - ELETTRONICO. - 173:(2026), pp. 1-18.

Availability:
This version is available at: 11583/3006828 since: 2026-01-22T10:58:10Z

Publisher:
Elsevier

Published
DOI:

Terms of use:

This article is made available under terms and conditions as specified in the corresponding bibliographic description in the repository

Publisher copyright

(Article begins on next page)

18 November 2026

Journal of the Mechanical Behavior of Biomedical Materials 173 (2026) 107205



Contents lists available at ScienceDirect

Journal of the Mechanical Behavior of Biomedical Materials

journal homepage: www.elsevier.com/locate/jmbbm





Mechanical characterization and constitutive modelling of commercial biopolymers and their blends for biomedical applications

Vito Burgio *, Martina Di Giacinti, Mariana Rodriguez Reinoso, Valentina Tuveri, Paola Antonaci, Cecilia Surace

BIO-MAterials and STructures Laboratory (BIOMAST Lab), Department of Structural, Geotechnical and Building Engineering, Politecnico di Torino, Corso Duca degli Abruzzi 24, 10129, Torino, Italy

A R T I C L E I N F O

Keywords:
Constitutive modelling
Biopolymers
Viscoplastic materials
Resomer
Three network model
Three network viscoplastic model
Flow evolution network
Constitutive laws

A B S T R A C T

Nowadays, biopolymers like Poly(lactic acid) (PLA) and Polycaprolactone (PCL) are commonly adopted in several fields of medicine, from orthopaedics to pharmacology. When dealing with medical applications like prostheses or scaffolds, it is crucial to have a deep knowledge of the mechanical properties of such biopolymers. Both biopolymers show a viscoplastic behaviour, namely, their mechanical response depends on the temperature and the velocity at which the loading or the deformation is applied. Currently, several companies commercialise a large variety of PCL and PLA blends with different ratios classified as "medical grade", indicating that such blends are suitable for manufacturing medical devices. The information about the mechanical behaviour of these blends remains unclear, since the datasheets available report information about the Young's Modulus, a limited amount of data considering their full mechanical behaviour. Most of these commercially available biopolymers have not been investigated thoroughly in the past. In this paper two commercially available biopolymers, Resomer® LR 704 S and LC 703 S, from Evonik were investigated. Specifically, the original polymers and the following blend combinations were tested: 60:40, 40:60, and 50:50. The original biopolymers and their blend combinations were considered to explore the application of developing two innovative devices for soft tissues repair, T-REMEDIE for tendon repair (Tendon Repair Medical DevIcE) [patent ID: IT202000006967A1]("Device and assembly for the repair of soft tissues, such as tendons and ligaments," 2020) and T-SURE for abdominal hernia repair (Tissue Surgical REpair), under development in the BIOMAST Lab (BIO-MAterials and STructures Laboratory) at the Politecnico di Torino. Experimental tensile tests on dog bone specimens manufactured by compression and injection moulding were evaluated. Based on the experimental results, the constitutive three network model (TNM), the three network viscoplastic (TNV) model and the Flow Evolution Network (FEN) model were implemented in MATLAB and calibrated. This work represents the first time these constitutive laws have been applied to biopolymers. All the models are suitable for biopolymer constitutive modelling, showing promising results. The constitutive material parameters for all the models are reported in the paper.

Glossary

λ = Stretch ratio
$\boldsymbol{F}$ = Deformation gradient
$\boldsymbol{F}^{-1}$ = Inverse of the deformation gradient
$\boldsymbol{F}^{T}$ = Transpose of the deformation gradient
$\boldsymbol{F}^{e}$ = Elastic part of the deformation gradient
$\boldsymbol{F}^{v}$ = Viscous part of the deformation gradient
$J = determinant(\boldsymbol{F})$ = determinant of Jacobian
$\boldsymbol{I}$ = Identity tensor
$\boldsymbol{b} = \boldsymbol{F}\boldsymbol{F}^{T}$ left Cauchy-Green tensor

(*continued on next column*)

(*continued*)

$\boldsymbol{b}^{*}$ = distortional part of the left Cauchy-Green tensor
$\boldsymbol{C} = \boldsymbol{F}^{T}\boldsymbol{F}$ right Cauchy-Green tensor
$\boldsymbol{C}^{*}$ = distortional part of the right Cauchy-Green tensor
$I_1(\boldsymbol{C})$ = first invariant of the right Cauchy-Green tensor
$\lambda_1, \lambda_2, \lambda_3$ = principal directions of the right Cauchy-Green tensor
$\boldsymbol{\sigma}$ = Cauchy stress tensor
$\boldsymbol{P}$ = Engineering stress or First Piola-Kirchhoff stress tensor
$\boldsymbol{L}$ = Velocity gradient
$\boldsymbol{D}$ = Rate of deformation tensor of the velocity gradient
$\boldsymbol{W}$ = Spin tensor of the velocity gradient

(*continued on next page*)

* Corresponding author.
E-mail address: vito.burgio@polito.it (V. Burgio).

https://doi.org/10.1016/j.jmbbm.2025.107205
Received 4 June 2025; Received in revised form 1 September 2025; Accepted 16 September 2025
Available online 17 September 2025
1751-6161/© 2025 The Authors. Published by Elsevier Ltd. This is an open access article under the CC BY-NC-ND license (http://creativecommons.org/licenses/by-nc-nd/4.0/).

(*continued*)

$\boldsymbol{N}$ = Direction of the driving deviatoric stress
$\dot{\boldsymbol{F}}$ = Time derivative of the deformation gradient

1. Introduction

The application of advanced non-linear constitutive models in the biomedical field paves the way for designing a new class of medical devices for improving patient's outcome. These advanced formulations increase the predictive power of numerical models, such as, finite element models. Finite Element Analysis (FEA) enables to predict the behaviour of the devices and the tissues around them under physiological or non-physiological working conditions, preventing complications. Interest in simulating medical devices has grown substantially in recent years since, from the regulatory (Food and Drug Administration (FDA) and European Medical Device Regulation (EU MDR)) prospective, numerical simulations are necessary for evaluating medical device performance and reliability. Furthermore, numerical simulation supports the 3Rs principle, Replacement, Reduction and Refinement of the use of animal models in scientific research and preclinical studies (Carniel et al., 2020). This leads to the creation of high-fidelity models that enhance the ability to predict their mechanical behaviour. Computational models have been developed, e.g., to gain a comprehensive understanding of stomach physiology. These models have proven valuable in preoperative planning, allowing for the analysis of potential outcomes across different surgical approaches (Berardo et al., 2024; Fontanella et al., 2019).

Biopolymers play a pivotal role in the field of biomedical engineering due to their inherent biocompatibility and biodegradability. The development of scaffolds and implantable devices requires the selection of appropriate biopolymers that can adequately meet the specific demands of the implantation site. To this end, biopolymers are frequently blended to achieve tailored mechanical and thermal properties (Bogdanov et al., 1998). Numerous studies have explored the use of biopolymers in scaffolds, drug delivery devices, orthopaedic fixation systems (screws, pins, and rods) (Stewart et al., 2018).

The numerical simulation of medical devices under physiological or unphysiological conditions represents a challenge, starting with evaluating the right material model. Materials involved in medical device fabrication range from stainless steel, titanium, nitinol, to various biocompatible polymers, including polyethylene, nylon, and biodegradable polymers like PLA and PCL. It is difficult to accurately simulate the behaviour of biopolymers in medical devices through computational modelling because of their viscoplastic mechanical behaviour. Nevertheless, the mechanical response of such materials has often been represented using traditional constitutive models leading to unsatisfactory results. These limitations have driven the development of new constitutive models designed to better capture the behaviour of thermoplastic polymers, which are frequently used for biomedical applications. Models like the TNM, TNV, and FEN have demonstrated excellent accuracy in simulating thermoplastic polymer behaviour. However, these advanced models remain rarely used, with only a limited number of articles in the literature referencing their application, and, unfortunately, no studies have explored their use with biocompatible and biodegradable polymers.

Implantable devices are exposed to various loading states in-vivo, such as shear, creep and cyclic loading. Finite element modelling provides a powerful tool for investigating their mechanical performance under both physiological and non-physiological conditions encountered at the implantation site. However, obtaining reliable and realistic results critically depends on the appropriate selection of constitutive models for the materials involved (soft tissues, biopolymers, and metals). It has been demonstrated that standard plasticity models, such as J_2-plasticity model, do not accurately capture the complex behaviour of thermoplastic polymers and consequently biopolymers (Bergstrom et al., 2002). For this reason, alternative models have been recently developed, such as (Anssari-Benam, 2024a, 2024b), that also cover applications to modelling the finite deformation under varying crystallinity ratios and deformation rates (Anssari-Benam and Zaïri, 2025).

In addition, the Three Network Model (TNM) was developed for the constitutive modelling of ultra-high molecular weight polyethylene (UHMWPE) (Bergström and Bischoff, 2010). In this application the model was calibrated on uniaxial tension, compression and cyclic data and then validated in a finite element model of the small punch test, showing an accurate prediction of the large-strain non-linear response.

The TNM was tested in high strain rate conditions to simulate polyether ether ketone (PEEK) during an impact scenario, the model showed a good approximation of the experimental results (Bergstrom et al., n.d.). The accuracy of the model was also tested in the predicting PEEK behaviour under multiaxial loading conditions using two experimental approaches: the small punch test and the spherical indentation test (Quinn et al., 2013). The ability of the model in prediction of scratch simulations was also evaluated on different thermoplastics (Diehl et al., 2013). Furthermore the TNM has been applied to make significant advancements in experimental fracture mechanics and in the tearing analysis of thin polymer films (Furmanski, 2022).

The reliability of the TNM model was also tested in simulating the post-yield strain-softening characteristics under large deformation of reinforced polymer composites. The numerical results from Kumar et al. (2022) show an excellent prediction of the behaviour of composite material filled with spherical particles and milled fibre epoxy (Kumar et al., 2022). The TNM was also use in the field of micromechanical model for composite materials using Representative volume elements (RVEs) (Laudon and Romanowicz, 2012).

Nevertheless, although the response of thermoplastic polymers is well captured by the TNM model, a new constitutive model called Three Network Viscoplastic (TNV) model was developed. Pratik and Powar (2021) adapted the TNV model, while investigating the effect of strain rate and anisotropy on low density polyethylene (LDPE) under monotonic and cyclic conditions (Pratik and Powar, 2021). In this case, the TNV model was capable of capturing the anisotropic response of LDPE with a 3.0 % error. However, different temperatures compared to room temperature were not tested (Pratik and Powar, 2021). Heiml and Kepler (2021) used the TNV model for evaluating 3D-printed cellular polymeric shoe soles (Heiml and Kepler, 2021). Almomani et al. (2023) applied the TNV model to investigate the prediction capability of the model for high density polyethylene (HDPE) under monotonic and cyclic loads (Almomani et al., 2023).

Following the theory of the previous two constitutive models, the Flow Evolution Networks (FEN) model was developed to simulate the stress–strain behaviour of poly(L-lactide) (PLLA), incorporating viscoplastic effects and the ability to model strong postyield softening (Dreher et al., 2017). The model was calibrated on specimens of PLLA, evaluating the mechanical behaviour in a fluid bath (physiologic testing conditions) and then evaluated to predict the force-displacement response of the unit cell of cardiovascular stents (Dreher et al., 2017). The ability to predict the experimental result of the FEN was also evaluated by modelling 30 % glass-fiber filled Polyetherimide (PEI) during three-point bending tests. The model was calibrated using uniaxial compression tests at lower and higher strain rates, uniaxial tension tests, and then the FEN model for the material was used to simulate three-point bending showing agreement with experimental data (Teller and Bergstrom, 2018).

The BIOMAST Lab at Politecnico di Torino is developing two innovative implantable devices: **T-REMEDIE** [patent ID: IT202000006967A1], designed for Achilles and hand tendon repair, and **T-SURE** (patent pending), intended for abdominal hernia repair. A critical step is the selection of suitable commercially available biopolymers. However, the information typically provided in material datasheets is insufficient, particularly due to the limited experimental campaign, unable provide information about the complex viscoplastic

behaviour exhibited by these materials. Starting from this limitation, the objective of this work was to experimentally assess the mechanical response of selected commercially available biopolymers and their blends, and provide constitutive models using the **TNM**, **TNV**, and **FEN** model for their application in FEA of medical devices. This research aims to provide a valuable reference for other researchers, startups, and medical device developers working toward innovative solutions to address unmet clinical needs.

Specifically, the present investigation focuses on the following biopolymers produced by Evonik:

- Resomer® LR 704 S, composed of two enantiomers of lactic acid with concentrations of 70:30 respectively of poly(L-lactide) (PLLA) and poly(D-lactide) (PDLA), called Poly-(L-Lactide-co-D,L-lactide)) or PLDLLA. Isotactic PLLA is the most commonly available type of PLA, characterized by transparency and a crystalline structure in which molecules are regularly arranged, which presents favourable mechanical properties and hardness. Generally, PLA is a brittle material with less than 10 % elongation at break, a slow degradation rate (approximately two years) due to lack of reactive side-chain group and hydrophobicity (Farah et al., 2016). However, the properties of PLA can be altered through various methods, such as adjusting the L/D ratio of isomers or copolymerizing it with other monomers, like PGA (Polyglicolic Acid) and PCL (Polycaprolactone) (Zhao and Zhao, 2016);
- Resomer® LC 703 S, composed of two different polymers, PLLA and poly(ε-caprolactone), with concentrations of 70:30 respectively. In literature, the mixture of these two polymers is called Poly(L-lactide-co-ε-caprolactone) or PLCL. Also, regarding PCL, the mechanical and thermal properties are closely dependent on molecular weight and degree of crystallinity. Its use is also found in the biomedical field with a degradation rate of about 1–2 years. Typically, PCL is not utilized alone in applications requiring structural integrity, as its plastic nature renders it unsuitable for such purposes. The application of PCL in combination with PLA is often used to combine the breaking strength of PLA with the much more elastic properties of PCL, also increasing its elongation at break (Guarino et al., 2017). Numerous investigations have been undertaken to explore PLCL copolymers. They display shorter degradation times, typically spanning from six to twelve months, along with varying degrees of stiffness and Young's modulus based on the respective proportions of its constituent polymers (Li et al., 2020). Literature suggests that the copolymer manifests thermoplastic-elastomeric behaviour, accompanied by notable elongation at break and impressive elastic recovery (Ugartemendia et al., 2018).

And the following blend of these two commercially available biopolymers:

- Resomer® LR 704 S - Resomer® LC 703 S ratio 60:40;
- Resomer® LR 704 S - Resomer® LC 703 S ratio 40:60;
- Resomer® LR 704 S - Resomer® LC 703 S ratio 50:50.

Furthermore, the TNM, TNV, and FEN models were originally developed for standard polymers and have not yet been evaluated for their applicability to biopolymers. This work is among the first studies to apply these models to biopolymer modelling. The material parameters of the constitutive laws are provided to facilitate their adoption by other researchers worldwide for numerical simulations to evaluate medical devices.

2. Materials and methods

The following subsections provide information on the commercially available biopolymers and their blend, the mechanical characterization tests, and the constitutive laws.

2.1. Medical-grade copolymers

The biodegradable medical-grade copolymers used in this study were supplied by Evonik Industries (Essen; www.evonik.com). This work is closely related to a previous study in which the effect of the manufacturing process was evaluated to assess the resulting mechanical properties (Reinoso et al., 2021). To evaluate the mechanical properties of each polymer and blend under investigation, dog-bone specimens Type 5A (specimen design according to ISO 527-2 standard) for Compression Moulding (CM) were manufactured. Following the evaluation of the mechanical properties of the biopolymers and their blend for CM, additional specimens of the Resomer® LR 704 S and Resomer® LC 703 S blend, in a 50:50 ratio, were produced using Injection Moulding (IM), the most common manufacturing technique for medical devices production.

2.1.1. Blend Resomer® LR 704 S - Resomer® LC 703 S

The creation of the polymer blend was carried out to combine the best properties of the individual biopolymers. Several research studies have explored polymer blends comprising PLA and PCL, examining their thermal, mechanical, morphological properties, and biodegradation. From a mechanical perspective, the addition of PLCL to PLDLLA causes a radical change in the biopolymer's behaviour, transforming it from a brittle material into a material more similar to thermoplastic rubbers with ductile behaviour (Ugartemendia et al., 2018). The blend compositions investigated in this study were selected based on a comprehensive review of the mechanical properties reported in the literature. Specifically, the original polymers and the following polymer blend ratios were examined: PLDLLA/PLCL 60:40, 40:60, and 50:50.

2.2. Mechanical characterization test

The mechanical characterization of all the commercially available biomedical polymers was conducted following the uniaxial tensile testing method described in ISO 527–1 for plastics. The machine used for the tests was an MTS Insight® Electromechanical Testing Systems with a load cell of 1000 N. A distance between grips of 30 mm, sampling frequency of 30 Hz, a constant cross-sectional region length 20 mm (L_0), and constant deformation speed of 0.5 mm/min were set. During the tests, force and displacement values were recorded using the Test Works® Software-MTS Systems Corporation.

Mechanical properties such as Young's Modulus, yield stress and strain, and stress and strain at failure were calculated based on engineering stress and engineering strain quantities. The Young's modulus for each biopolymer was calculated within an engineering strain range of 0.01–0.04 as reported in ISO 527–1. Additionally, a MATLAB script was developed to measure the error introduced when the material is assumed to behave as a linear elastic material. The elastic behaviour limit defines the maximum engineering strain that can be considered when modelling the material with a linear elastic model using Young's modulus. Specifically, the code evaluates the percentage difference between the Young's modulus and the local slope of the stress–strain curve, identifying the strain at which this difference exceeds 30 %. Hence, the elastic behaviour limit corresponds to the engineering strain value at which the error introduced by modelling the material as linear elastic exceeds 30 %.

The experimental data are presented in the figures as either Engineering Stress, or considering the theory of finite deformation, the first Piola-Kirchhoff stress tensor ($\boldsymbol{P}$) or Engineering stress (Holzapfel, 2002; J.S. Bergstrom, 2015), versus Engineering strain ($\varepsilon_{eng} = \frac{\Delta l}{L_0}$), True Stress versus Engineering Strain or True Stress versus Logarithmic Strain or true strain ($\varepsilon_{ln} = \ln\left(1 + \varepsilon_{eng}\right)$).

2.3. Constitutive modelling formulation

The following subsections delve into the constitutive laws assessed for their application to the selected biopolymers.

2.3.1. Three network model (TNM)

The standard configuration of this model is represented as a three-network acting in parallel. Two of these networks are composed of a non-linear spring and a non-linear dashpot, the third network presents only a non-linear spring (see Fig. 1). The initial viscoplastic response is captured using two separate energy activation mechanisms, corresponding to amorphous and semicrystalline domains, and the large strain response is controlled by entropic resistance (Bergström and Bischoff, 2010).

In this model framework, the deformation gradient $\boldsymbol{F}$ acts equally in each network. In the network A and B the deformation gradient is multiplicatively decomposed into elastic and viscoplastic components: $\boldsymbol{F_n} = \boldsymbol{F_n^e F_n^v}$ (n = networks A and B respectively). Usually, the non-linear spring behaviour is modelled using the Eight Chain model (Arruda and Boyce, 1992). An incompressible formulation was adopted. The Eight-Chain model is a hyperelastic model designed to describe the mechanical behaviour of rubber-like materials. Adopting this model the Cauchy stress acting on network A given by:

$$\boldsymbol{\sigma_A} = \frac{\mu_A}{J_A^e \overline{\lambda_A^e}}\left[1 + \frac{\theta - \theta_0}{\widehat{\theta}}\right]\frac{\mathscr{L}^{-1}\left(\frac{\overline{\lambda_A^e}}{\lambda^{lock}}\right)}{\mathscr{L}^{-1}\left(\frac{1}{\lambda^{lock}}\right)} dev\left[\boldsymbol{b_A^e}\right] - p\boldsymbol{I} \tag{1}$$

Where $\boldsymbol{b_A^e} = \boldsymbol{F_A^e}^T \boldsymbol{F_A^e}$ is the elastic part of the left Cauchy-Green tensor, $\boldsymbol{I}$ is the identity tensor, $J_A^e = \det\left[\boldsymbol{F_A^e}\right]$ is the determinant of Jacobian, μ_A is the shear modulus of network A, $\overline{\lambda_A^e}$ is the effective chain stretch based on the eight-chain assumption (Arruda and Boyce, 1992) (see equation (2)), $\mathscr{L}^{-1}(x)$ is the inverse Langevin function ($\mathscr{L}(x) = coth(x) - 1$), λ^{lock} is the chain locking stretch, and p is an indeterminate Lagrangian multiplier, which can be identified as a hydrostatic pressure, θ is the current temperature, θ_0 is a reference temperature (thermal expansion reference temperature) and $\widehat{\theta}$ is a material parameter specifying the temperature response of the stiffness (temperature factor). The constitutive parameters of the non-linear elastic part are the μ shear modulus, $\widehat{\theta}$ the temperature response of the stiffness and thelimiting chain stretch λ^{lock}.

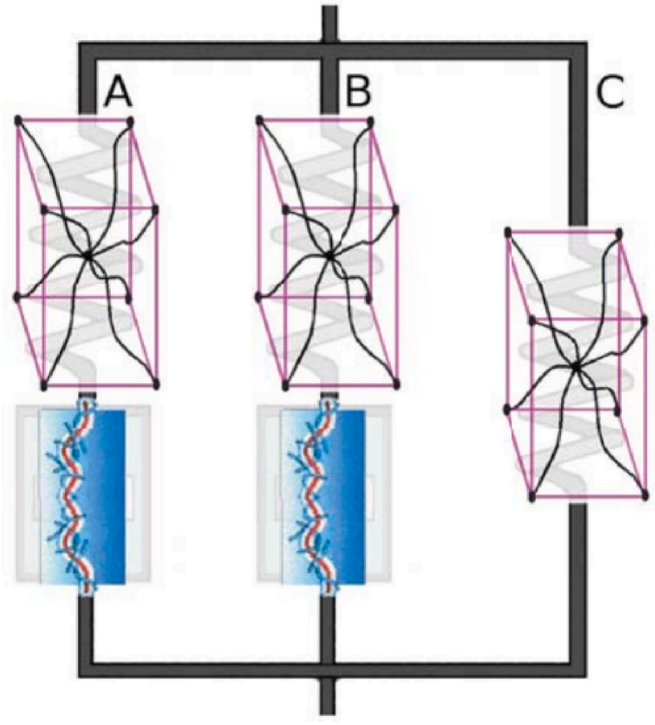


Fig. 1. Rheological representation of the TNM model (Bergström and Bischoff, 2010).

$$\overline{\lambda_A^{e^*}} = \left[\frac{\lambda_1^{e\,2} + \lambda_2^{e\,2} + \lambda_3^{e\,2}}{3}\right]^{\frac{1}{2}} = \sqrt{\frac{tr\boldsymbol{C_A^e}}{3}} = \sqrt{\frac{tr\boldsymbol{b_A^e}}{3}} = \sqrt{\frac{I_1^e}{3}} \tag{2}$$

Where $\boldsymbol{C_A^e} = \boldsymbol{F_A^e F_A^{eT}}$ is the elastic right Cauchy-Green tensor, I_1^e is the first invariant of $\boldsymbol{C_A^e}$ and $\lambda_1^e, \lambda_2^e, \lambda_3^e$ are the principal directions of $\boldsymbol{C_A^e}$. The Cauchy stress acting on network B has the same representation of network A. The only difference between network A and network B is that the shear modulus of network B is taken to evolve with plastic strain from an initial value μ_{Bi} to a final value μ_{Bf} according to:

$$\dot{\mu}_B = -\beta\left[\mu_{Bi} - \mu_{Bf}\right].\dot{\gamma}_A \tag{3}$$

Where β is the evolution rate of μ_B and $\dot{\gamma}_A$ is the viscoplastic flow rate or effective deviatoric flow rate of network A, that will be treated specifically in the following part. This evolution equation for μ_B enables the model to better capture the distributed yielding that is observed in many thermoplastics (J.S. Bergstrom, 2015). To complete the model, it is also necessary to specify the rate of change in the internal state of the material through kinematics rate equations of the model. The velocity gradient in network A is $\boldsymbol{L_A} = \dot{\boldsymbol{F}}_A \boldsymbol{F_A^{-1}}$ and can be decomposed into elastic and viscous components as follows:

$$\boldsymbol{L_A} = \boldsymbol{L_A^e} + \widetilde{\boldsymbol{L}}_A^{\boldsymbol{v}} \tag{4}$$

$$\widetilde{\boldsymbol{L}}_A^{\boldsymbol{v}} = \widetilde{\boldsymbol{D}}_A^{\boldsymbol{v}} + \widetilde{\boldsymbol{W}}_A^{\boldsymbol{v}} \tag{5}$$

Where $\widetilde{\boldsymbol{D}}_A^{\boldsymbol{v}}$ is the rate of viscous deformation of the velocity gradient $\widetilde{\boldsymbol{L}}_A^{\boldsymbol{v}}$. To make the unloading process unique the term $\widetilde{\boldsymbol{W}}_A^{\boldsymbol{v}}$ (the spin term) is set to zero.

The rate of viscous flow of network A $\widetilde{\boldsymbol{D}}_A^{\boldsymbol{v}}$ is given by equation (6), where $\dot{\gamma}_A$ is the effective deviatoric flow rate and $\boldsymbol{N_A^v}$ is the direction of the driving deviatoric stress of the relaxed configuration convected to the current configuration, and it is represented by $\boldsymbol{N_A^v} = \frac{dev[\sigma_A]}{\|dev[\sigma_A]\|_F}$, where the denominator of $\boldsymbol{N_A^v}$ define the effective stress driving the viscous flow by the Frobenius norm (in the following denoted by τ_A).

$$\widetilde{\boldsymbol{D}}_A^{\boldsymbol{v}} = \dot{\gamma}_A(\sigma_A, b_A^e)\boldsymbol{N_A^v} \tag{6}$$

Therefore, the time derivative of the deformation gradient of the viscoelastic flow $\dot{\boldsymbol{F}}_A^{\boldsymbol{v}}$ can be expressed by:

$$\dot{\boldsymbol{F}}_A^{\boldsymbol{v}} = \dot{\gamma}_A \boldsymbol{F_A^{e\,-1}} \frac{dev[\boldsymbol{\sigma_A}]}{\|dev[\boldsymbol{\sigma_A}]\|_F} \boldsymbol{F_A^e F_A^v} \tag{7}$$

The previous equation shows the relation of the time derivative of the deformation gradient based on pure kinematics considering only the physics, and the relation of the effective deviatoric flow rate is considered as a scalar equation. The equation for the effective deviatoric flow rate $\dot{\gamma}_A$ is governed by a micromechanism-inspired model that is responsible of the time-dependent behaviour.

$$\dot{\gamma}_A = \dot{\gamma}_0\left(\frac{\tau_A}{\widehat{\tau}_A + aR(p_A)} - \tau_c\right)^{m_A}\left(\frac{\theta}{\theta_0}\right)^n \tag{8}$$

In equation (8), $\dot{\gamma}_0 = 1/s$ is a constant introduced for dimensional consistency, $p_A = -[(\sigma_A)_{11} + (\sigma_A)_{22} + (\sigma_A)_{33}]/3$ is the hydrostatic pressure, $R(x) = (x + |x|)/2$ is a ramp function, τ_A is the effective shear stress, $\tau_c =$

0.01 is the limit such that flow only occurs when $\frac{\tau_A}{\widehat{\tau}_A + aR(p_A)} > \tau_c$, $\widehat{\tau}_A$ is the flow resistance, and m_A is the stress exponential. The parameter a is the pressure dependence of flow, which has a value between 0 and 1 and controls the triaxiality of the stress (need to be set at zero if there are only uniaxial tension and compression data for calibrating the model). The constitutive parameters of the effective deviatoric flow rate $\dot{\gamma}_A$ are the flow resistance $\widehat{\tau}_A$ and the stress exponential m_A. The same equations are adopted for network B. Network C comprises a nonlinear spring and does not include the nonlinear dashpot.

The total Cauchy stress in the system is given by the sum of the stresses in each network: $\boldsymbol{\sigma} = \boldsymbol{\sigma_A} + \boldsymbol{\sigma_B} + \boldsymbol{\sigma_C}$. The TNM implemented in this work has 10 material parameters that must be determined for the specific material under investigation (see Table 1).

For the model to be implemented effectively the parameters must be restricted to a specified range. The exponents m_A and m_B in the effective deviatoric flow rate must be less than 20 to ensure proper convergence. The flow resistance $\widehat{\tau}_A$ should be less than $\widehat{\tau}_B$ to ensure proper convergence. The initial shear modulus of network B μ_{Bi}, should be greater than the final shear stiffness μ_{Bf}.

2.3.2. Three network viscoplastic (TNV) model

The standard configuration of this model is represented as a three-network system acting in parallel; each of these networks is composed of a non-linear spring and a non-linear dashpot. The deformation gradient $\boldsymbol{F}$ acts equally in each network and can be multiplicatively decomposed into elastic and viscoplastic components: $\boldsymbol{F_n} = \boldsymbol{F_n^e F_n^v}$ (n = networks A, B and C respectively) (Almomani et al., 2023). Usually, the non-linear spring behaviour is modelled using an Eight-Chain model (see equation (1)).

The Cauchy stress acting on network B and C has the same form as that of network A. As in the TNM, the shear modulus of network B is taken to evolve with plastic strain from an initial value μ_{Bi} to a final value μ_{Bf} according to equation (3) reported previously. Instead, the shear modulus of network C remains constant throughout the deformation.

To complete the model, it is also necessary to specify the rate of change in the internal state of the material through the kinematics rate equations of the model. The velocity gradient in networks A, B and C is $\boldsymbol{L_N} = \dot{\boldsymbol{F}}_{\boldsymbol{N}} \boldsymbol{F}_{\boldsymbol{N}}^{-1}$ with N equal to A, B and C, and can be decomposed into elastic and viscous components as reported previously for the TNM model. Therefore, following the same process shown for the TNM model, the time derivative of the deformation gradient of the viscoelastic flow $\dot{\boldsymbol{F}}_{\boldsymbol{N}}^{\boldsymbol{v}}$ (with N equal to A, B and C) can be expressed by equation (7). The equation for the effective deviatoric flow rate $\dot{\gamma}_N$ (with N equal to A, B and C) is governed by a micromechanism-inspired model that describes the time-dependent behaviour and is shown in equation (8).

The total Cauchy stress in the system is given by the sum of the stresses in each network: $\boldsymbol{\sigma} = \boldsymbol{\sigma_A} + \boldsymbol{\sigma_B} + \boldsymbol{\sigma_C}$. The TNV implemented in this work has 12 material parameters that need to be determined for the specific material under investigation (see Table 2). The terms representing the effect of the temperature on the mechanical behaviour of the material have been omitted as all experiments were performed at room temperature. The same equations are adopted for all networks of the TNV model.

The parameters must be restricted to a specified range of values in order for the model to be implemented effectively. The exponent m_A, m_B and m_c in the effective deviatoric flow rate must be less than 20 to ensure proper convergence. The flow resistance $\widehat{\tau}_A$ should be less than $\widehat{\tau}_B$ and $\widehat{\tau}_B$ should be less than $\widehat{\tau}_C$ to ensure proper convergence. The initial shear modulus of network B μ_{Bi}, should be greater than the final shear stiffness μ_{Bf}.

2.3.3. FEN

The FEN model is a multi-network viscoplastic material model developed to represent the mechanical response of PLLA (Dreher et al., 2017). The rheological representation of the model is illustrated in Fig. 2. According to the original implementation, the model is based on two parallel networks, but additional parallel networks maybe adopted if necessary, based on the experimental data.

In this model framework, the deformation gradient $\boldsymbol{F}$ acts equally in each network. In the networks A and B the deformation gradient is multiplicatively decomposed into elastic and viscoplastic components: $\boldsymbol{F_n} = \boldsymbol{F_n^e F_n^v}$ (n = networks A and B respectively). In the original version of the FEN model the Cauchy stress in each network is given by a Neo-Hookean hyperelastic material model. The Cauchy stress in network A is modelled as:

$$\sigma_A = \frac{2C_{10}}{J_A^e} dev\left[\boldsymbol{b_A^e}\right] - p\boldsymbol{I} \tag{9}$$

Instead, in network B the Cauchy stress is modelled as:

$$\sigma_B = \frac{2f_B C_{10}}{J_B^e} dev\left[\boldsymbol{b_B^e}\right] - p\boldsymbol{I} \tag{10}$$

Where $\boldsymbol{b_A^e} = \boldsymbol{F_A^e}^{\boldsymbol{T}} \boldsymbol{F_A^e}$ is the elastic part of the left Cauchy-Green tensor, $\boldsymbol{I}$ is the identity tensor, $J_A^e = \det\left[\boldsymbol{F_A^e}\right]$ is the Jacobian, C_{10} is the shear modulus of network A [MPa] and p is an indeterminate Lagrangian multiplier, which can be identified as a hydrostatic pressure. Instead, $[C_{10}, f_B, k]$ are material parameters for the model.

It is possible to modify the model changing the hyperelastic model material. Usually, the non-linear spring behaviour is modelled using an Eight Chain model (Arruda and Boyce, 1992). According to the TNM and TNV formulation in the implementation of the FEN model the hyperelastic model adopted was the Eight Chain model (Arruda and Boyce, 1992). The Cauchy stress acting on networks A is reported in equation (1). The Cauchy stress acting on network B has the same representation

Table 1
Material parameters used by the TNM. The material parameters controlling the temperature dependence have been omitted since all experiments were performed at room temperature.

Symbol	Description
μ_A	Shear modulus of network A [MPa]
λ^{lock}	limiting chain stretch or locking stretch
$\widehat{\tau}_A$	flow resistance of network A [MPa]
m_A	Stress exponential of network A
$a = 0$	pressure dependence of flow
μ_{Bi}	Initial shear modulus of network B
μ_{Bf}	Final shear modulus of network B
β	evolution rate of μ_B
$\widehat{\tau}_B$	flow resistance of network B [MPa]
m_B	Stress exponential of network B
μ_C	Shear modulus of network C [MPa]

Table 2
Material parameters used by the TNV model. The material parameters controlling the temperature dependence have been omitted since all experiments were performed at room temperature.

Symbol	Description
μ_A	Shear modulus of network A [MPa]
λ^{lock}	limiting chain stretch or locking stretch
$\widehat{\tau}_A$	flow resistance of network A [MPa]
m_A	Stress exponential of network A
$a = 0$	pressure dependence of flow
μ_{Bi}	Initial shear modulus of network B
μ_{Bf}	Final shear modulus of network B
β	evolution rate of μ_B
$\widehat{\tau}_B$	flow resistance of network B [MPa]
m_B	Stress exponential of network B
μ_C	Shear modulus of network C [MPa]
$\widehat{\tau}_C$	flow resistance of network C [MPa]
m_C	Stress exponential of network C

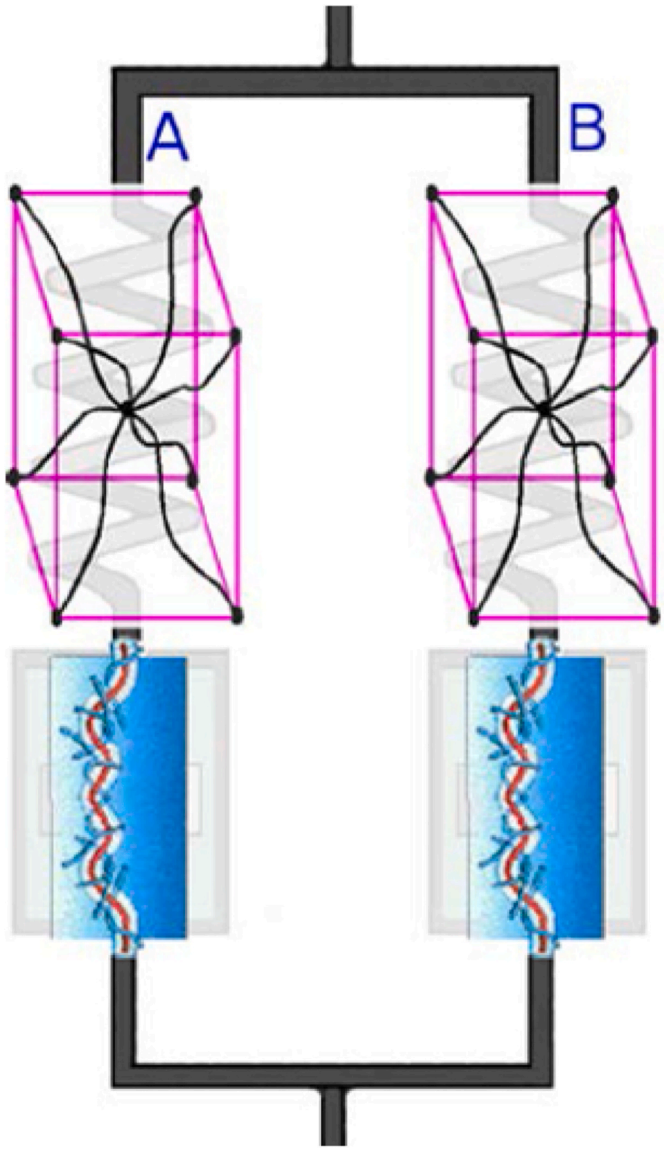


Fig. 2. Rheological representation of the Flow Evolution Network (Dreher et al., 2017).

of network A. The only difference between network A and network B is that C_{10} is multiplied by a factor f_B to scale the magnitude of the network B.

To complete the model, it is also necessary to specify the rate of change in the internal state of the material through the kinematics rate equations of the model. Therefore, following the same process shown for the TNM and TNV, the time derivative of the deformation gradient of the viscoelastic flow $\dot{\boldsymbol{F}}_{\boldsymbol{N}}^{\dot{\boldsymbol{\nu}}}$ (with N equal to A and B) can be expressed by equation (7). The equation for the effective deviatoric flow rate $\dot{\gamma}_A$ in the FEN model is:

$$\dot{\gamma}_A = \dot{\gamma}_0 \, R\left(\frac{\tau_A}{g_A^e \tau_A^h} - \tau_c\right)^{m_A} \tag{11}$$

Where $\dot{\gamma}_0 = 1/s$ is a constant introduced for dimensional consistency, $R(x) = (x + |x|)/2$ is a ramp function, $\tau_c = 0.001$, τ_A define the effective stress by the Frobenius norm, τ_A^h is the flow resistance, m_A is the stress exponential. The normalized τ_c and the ramp function were introduced to get a purely elastic response for very small strains (Dreher et al., 2017). The constitutive parameters of the effective deviatoric flow rate in each network are $[m_A, \tau_A^h]$. The factor g_A^e for network A, is capturing the yield evolution caused by the reduction in the activation energy spectrum after yielding:

$$\frac{dg_A^e}{dt} = \frac{1}{D_e}(g_{ss} - g_A^e)\dot{\gamma}_A \tag{12}$$

where are $[D_e, g_{ss}]$ material parameters (see Table 3). The same equations are adopted for network B. The total Cauchy stress in the system is given by the sum of the stresses in each network: $\boldsymbol{\sigma} = \boldsymbol{\sigma_A} + \boldsymbol{\sigma_B}$.

2.3.4. Material models calibration

The constitutive parameters were evaluated by comparing models and experimental uniaxial data by a fitting procedure using a Genetic Algorithm (GA) to explore all the possible combinations of the parameters. A specific MATLAB file for each model was made. The MATLAB file represents the analytical model to interpret the experimental tests accounting for the specific constitutive formulation and the specific boundary conditions that were implemented. Concerning uniaxial tensile tests, the analytical model provides a relationship between true stress along the loading direction and the imposed strain configuration. The material parameter determination was performed by minimising the following function:

$$GA\ minimisation\ function = \sum_{i=1}^{N} 100 \cdot \left(1 - \frac{\sigma_{11\ model}^N}{\sigma_{11\ experimental}^N}\right) \tag{13}$$

Where N are all the data points collected during the uniaxial tensile test. Eq. (13) provides a normalized point-to-point difference between experimental and numerical prediction, providing good calibration results.

3. Results

3.1. Mechanical characterization

The following subsections report the results of the uniaxial tensile test and the mechanical characterization of the biopolymers under investigation. It is important to point out that this behaviour is characteristic of this specific deformation rate (0.5 mm/min). Increasing or decreasing the deformation speed changes the behaviour of the polymer.

3.1.1. Resomer® LR 704 S, Poly(L-lactide-co-D,L-lactide) CM

The uniaxial tensile test performed on dog bone specimens of Resomer® LR 704 S manufactured by CM shows a linear elastic behaviour with a brittle fracture behaviour. Fig. 3 shows the true stress (continuous) and engineering stress (dotted) – strain curves resulting from the uniaxial tensile tests. Table 4 shows the mechanical parameters calculated on the experimental data.

3.1.2. Resomer® LC 703 S, Poly(L-lactide-co-ε-caprolactone) CM

The uniaxial tensile test performed on dog bone specimens of Resomer® LC 703S manufactured by CM shows an initial linear elastic response followed by yielding and then strain hardening at large

Table 3
Material parameters used by the FEN model. The material parameters controlling the temperature dependence have been omitted since all experiments were performed at room temperature.

Symbol	Description
C_{10}	Shear modulus of network A [MPa]
f_B	Multiplicative factor to scale the magnitude of the network B
$\widehat{\tau}_A$	flow resistance of network A [MPa]
m_A	Stress exponential of network A
$\widehat{\tau}_B$	flow resistance of network B [MPa]
m_B	Stress exponential of network B
D_e	Material parameter that regulates the evolution of g_A^e
g_{ss}	Material parameter that regulates the evolution of g_A^e

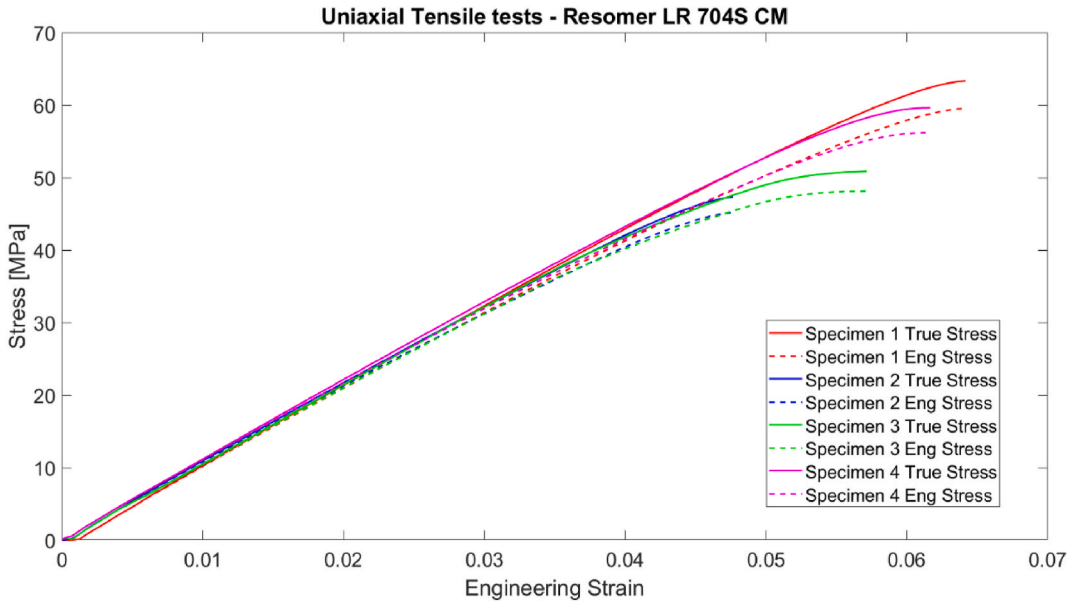


Fig. 3. Uniaxial tensile test results on Resomer® LR 704 S made by CM.

Table 4
– Mechanical parameters calculated from the uniaxial tensile test of Resomer® LR 704 S made by CM.

	Young's Modulus [MPa]	Elastic Behaviour Limit[a]	Yielding Stress[b] [MPa]	Yielding Strain[b]	Stress at Failure[b] [MPa]	Strain at Failure[b]
Specimen 1	1060.10	0.056	//	//	59.51	0.06
Specimen 2	1018.47	0.044	//	//	45.17	0.05
Specimen 3	1040.36	0.042	//	//	48.12	0.06
Specimen 4	1043.87	0.052	//	//	56.18	0.06
Mean ± standard deviation	1040.60 ± 17.01	0.049 ± 0.01	//	//	52.25 ± 6.71	0.058 ± 0.01

[a] The elastic behaviour limit defines the maximum engineering strain that can be considered when modelling the material with a linear elastic model.
[b] All the stress and strain are engineering quantities.

deformations. It is important to note that this behaviour is specific to the deformation speed of 0.5 mm/min. Increasing or decreasing the deformation speed changes the behaviour of the polymer. Specimen 2 exhibits a different behaviour compared to the other specimens; therefore, it is excluded from the following analysis.

Fig. 4 shows the true stress (continuous) and engineering stress (dotted) – strain curves resulting from the uniaxial tensile tests. Table 5 shows the mechanical parameters calculated on the experimental data.

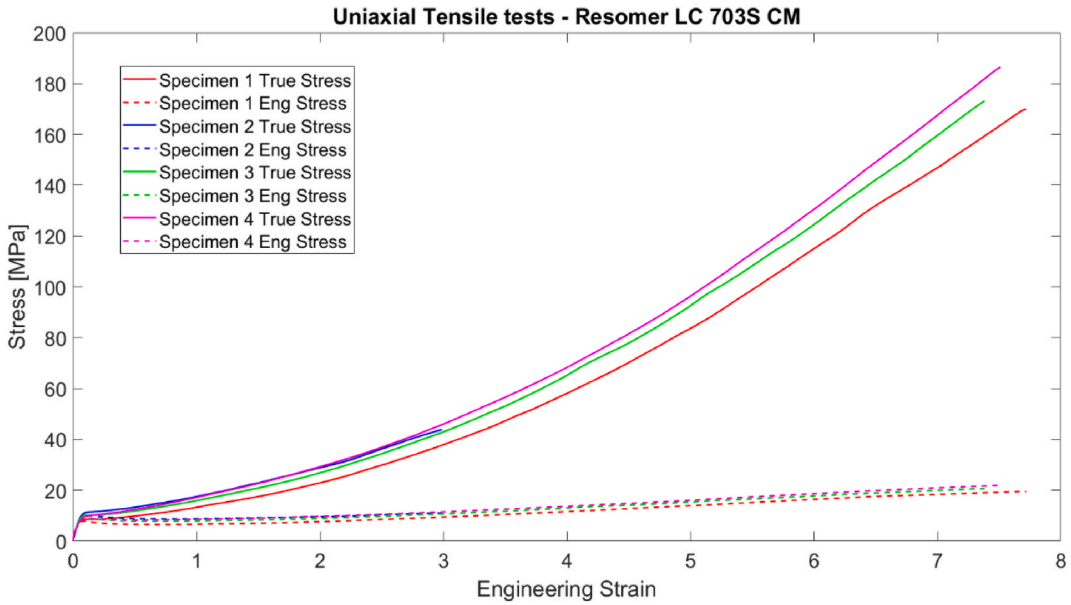


Fig. 4. Uniaxial tensile test results on Resomer® LC 703 S made by CM.

Table 5
Mechanical parameters calculated from the uniaxial tensile test of Resomer® LC 703 S made by CM.

	Young's Modulus [MPa]	Elastic Behaviour Limit[a]	Yielding Stress[b] [MPa]	Yielding Strain[b]	Stress at Failure[b] [MPa]	Strain at Failure[b]
Specimen 1	116.39	0.04	7.86	0.09	19.48	7.70
Specimen 3	128.41	0.05	9.27	0.09	17.74	5.98
Specimen 4	120.54	0.05	//	//	21.72	7.39
Mean ± standard deviation	121.79 ± 6.10	0.04 ± 0.00	8.57 ± 1.00	0.09 ± 0.00	19.65 ± 1.99	7.03 ± 0.92

[a] The elastic behaviour limit defines the maximum engineering strain that can be considered when modelling the material with a linear elastic model.
[b] All the stress and strain are engineering quantities.

3.1.3. Blend Resomer® LR 704 S - Resomer® LC 703 S

The following subsections report the results of the uniaxial tensile test and the mechanical characterization of different blend ratios of the original biopolymers.

3.1.3.1. Blend Resomer® LR 704 S - Resomer® LC 703 S ratio 60:40 CM. The uniaxial tensile tests performed on dog bone specimens of blend of Resomer® LR 704 S - Resomer® LC 703 S ratio 60:40 manufactured by CM shows an initial linear elastic response followed by yielding and then a softening behaviour until failure. Fig. 5 shows the true stress (continuous) and engineering stress (dotted) – strain curves resulting from the uniaxial tensile tests. Table 6 shows the mechanical parameters calculated fitting the experimental data.

3.1.3.2. Blend Resomer® LR 704 S - Resomer® LC 703 S ratio 50:50 CM. The uniaxial tensile test performed on dog bone specimens of blend of Resomer® LR 704 S - Resomer® LC 703 S ratio 50:50 manufactured by CM, shows an initial linear elastic response followed by yielding and then a strain hardening behaviour until failure. Fig. 6 shows the true stress (continuous) and engineering stress (dotted) – strain curves resulting from the uniaxial tensile tests. Table 7 shows the mechanical parameters calculated fitting the experimental data.

3.1.3.3. Blend Resomer® LR 704 S - Resomer® LC 703 S ratio 40:60 CM. The uniaxial tensile test performed on dog bone specimens of blend of Resomer® LR 704 S - Resomer® LC 703 S ratio 40:60 manufactured by CM shows an initial linear elastic response followed by yielding and then a strain hardening behaviour until failure. Specimen 4 exhibits a different behaviour compared to the other specimens; therefore, it is excluded from the following analysis. Fig. 7 shows the true stress (continuous) and engineering stress (dotted) – strain curves resulting from the uniaxial tensile tests. Table 8 shows the mechanical parameters calculated fitting the experimental data.

3.1.3.4. Blend Resomer® LR 704 S - Resomer® LC 703 S ratio 50:50 IM. The uniaxial tensile test performed on dog bone specimens of blend of Resomer® LR 704 S - Resomer® LC 703 S ratio 50:50 manufactured by IM shows an initial linear elastic response followed by yielding and then a strain hardening behaviour until failure. Fig. 8 shows the true stress (continuous) and engineering stress (dotted) – strain curves resulting from the uniaxial tensile tests. Table 9 shows the mechanical parameters calculated fitting the experimental data.

3.2. Constitutive modelling

The following subsections present the results of the constitutive model calibration for the evaluated viscoplastic materials.

3.2.1. Constitutive modelling Resomer® LC 703 S CM

The following subsections report the results of the numerical calibration of the two constitutive models under investigation, the TNM and TNV model, to simulate dog-bone specimens of Resomer® LC 703 S manufactured by CM.

3.2.1.1. TNM. The calibration of the TNM model on specimens of Resomer® LC 703 S manufactured by CM yielded optimal results. Considering the whole range of deformation, the calibrated model slightly overestimates the true stress of the biopolymer near the failure point. Fig. 9 shows the experimental true stress (continuous) and numerical true stress (dotted). Table 10 reports the TNM constitutive parameters obtained for each specimens evaluated.

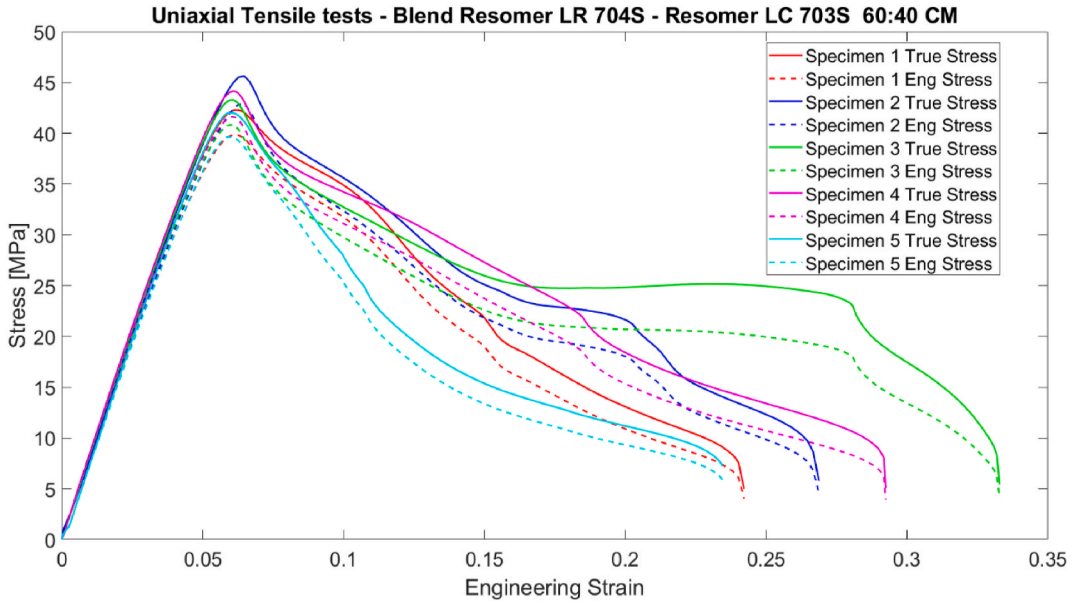


Fig. 5. – Uniaxial tensile test results on blend of Resomer® LR 704 S - Resomer® LC 703 S ratio 60:40 made by CM.

Table 6
Mechanical parameters calculated from the uniaxial tensile test of blend of Resomer® LR 704 S - Resomer® LC 703 S ratio 60:40 made by CM.

	Young's Modulus [MPa]	Elastic Behaviour Limit[a]	Yielding Stress[b] [MPa]	Yielding Strain[b]	Stress at Failure[b] [MPa]	Strain at Failure[b]
Specimen 1	755.04	0.05	39.84	0.06	4.02	0.2422
Specimen 2	769.63	0.05	42.85	0.06	4.57	0.2687
Specimen 3	742.94	0.05	40.82	0.06	4.07	0.3329
Specimen 4	778.96	0.05	41.62	0.06	3.94	0.2925
Specimen 5	774.22	0.05	39.65	0.06	5.86	0.2345
Mean ± standard deviation	746.16 ± 14.86	0.05 ± 0.00	40.96 ± 1.32	0.06 ± 0.00	4.49 ± 0.80	0.27 ± 0.04

[a] The elastic behaviour limit defines the maximum engineering strain that can be considered when modelling the material with a linear elastic model.
[b] All the stress and strain are engineering quantities.

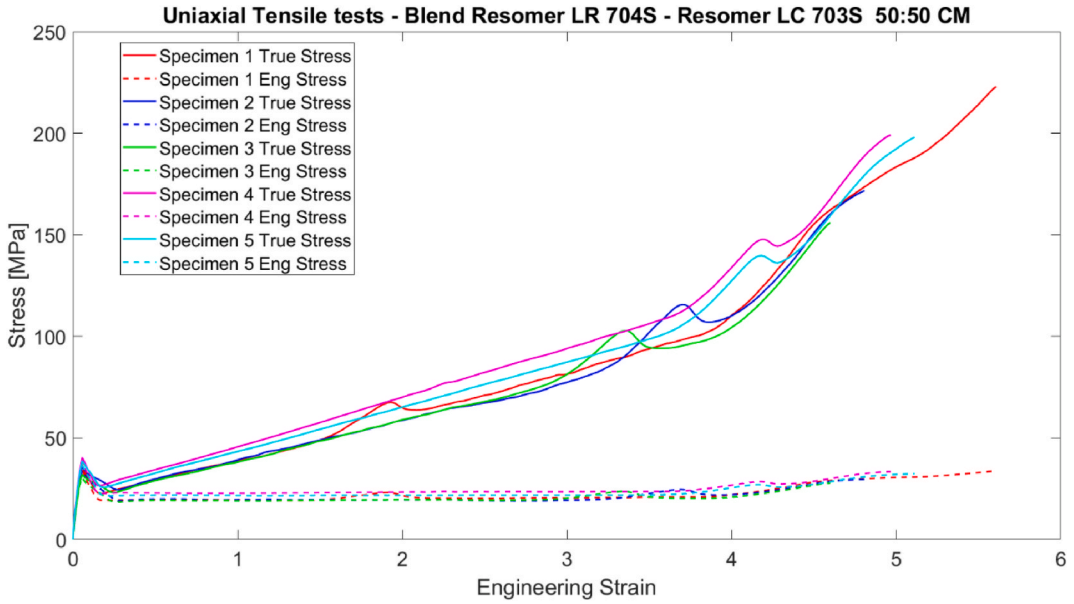


Fig. 6. Uniaxial tensile test results on blend of Resomer® LR 704 S - Resomer® LC 703 S ratio 50:50 made by CM.

Table 7
Mechanical parameters calculated from the uniaxial tensile test of blend of Resomer® LR 704 S - Resomer® LC 703 S ratio 50:50 made by CM.

	Young's Modulus [MPa]	Elastic Behaviour Limit[a]	Yielding Stress[b] [MPa]	Yielding Strain[b]	Stress at Failure[b] [MPa]	Strain at Failure[b]
Specimen 1	625.44	0.06	35.27	0.06	33.73	5.61
Specimen 2	626.71	0.06	33.99	0.06	29.57	4.81
Specimen 3	575.05	0.04	30.27	0.06	27.86	4.60
Specimen 4	649.81	0.06	38.22	0.06	33.36	4.97
Specimen 5	641.20	0.06	36.57	0.06	32.40	5.11
Mean ± standard deviation	623.64 ± 29.01	0.05 ± 0.02	34.86 ± 3.00	0.06 ± 0.00	31.38 ± 2.56	5.02 ± 0.38

[a] The elastic behaviour limit defines the maximum engineering strain that can be considered when modelling the material with a linear elastic model.
[b] All the stress and strain are engineering quantities.

3.2.1.2. TNV. Compared to the TNM model, the TNV model accurately captures the yielding point and slightly overestimates the true stress value near the failure point. However, the prediction is extremely accurate. Fig. 10 shows the experimental true stress (continuous) and numerical true stress (dotted). Table 11 reports the TNV constitutive parameters obtained for each specimens evaluated.

3.2.2. Constitutive modelling Blend Resomer® LR 704 S - Resomer® LC 703 S ratio 40:60 CM

The following subsections report the results of the numerical calibration of the two constitutive models under investigation, the TNM and TNV model, to simulate dog-bone blend specimens with a ratio 40:60 of Resomer® LR 704 S - Resomer® LC 703 S manufactured by CM.

3.2.2.1. TNM. The calibration of TNM model on blend specimens with a ratio 40:60 of Resomer® LR 704 S - Resomer® LC 703 S manufactured by CM yielded optimal results. Fig. 11 shows the experimental true stress (continuous) and numerical true stress (dotted). Table 12 reports the TNM constitutive parameters obtained for each specimens evaluated.

3.2.2.2. TNV. Compared to the TNM model, the prediction of the TNV model is accurate as well. Fig. 12 shows the experimental true stress (continuous) and numerical true stress (dotted). Table 13 reports the TNV constitutive parameters obtained for each specimens evaluated.

3.2.3. Constitutive modelling Blend Resomer® LR 704 S - Resomer® LC 703 S ratio 50:50 CM

The following subsections report the results of the numerical calibration of the two constitutive models under investigation, the TNM and TNV model, to simulate dog-bone blend specimens with a ratio 50:50 of Resomer® LR 704 S - Resomer® LC 703 S manufactured by CM.

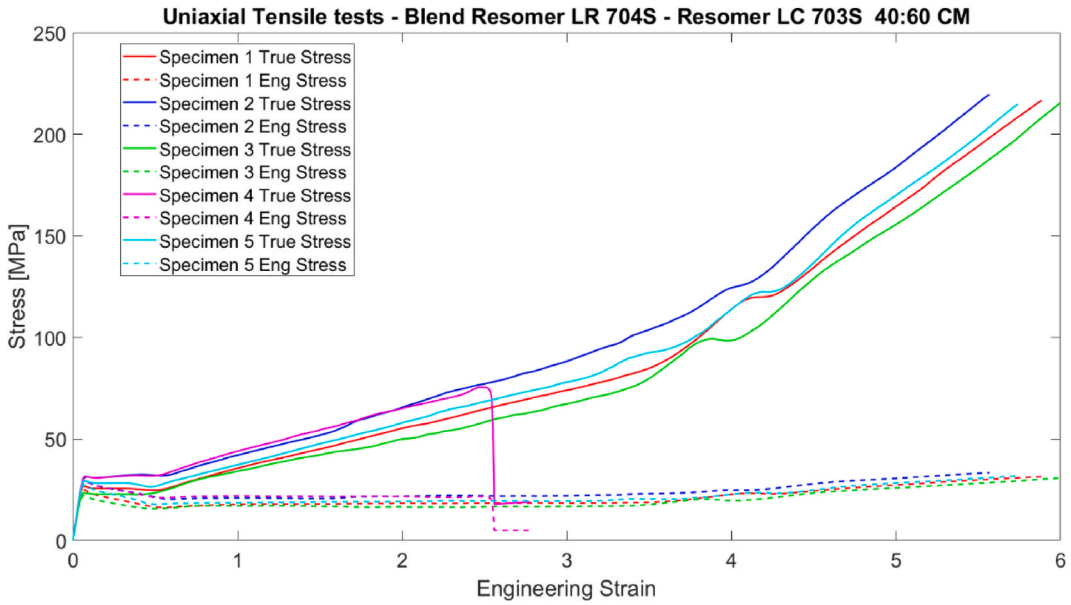


Fig. 7. – Uniaxial tensile test results on blend of Resomer® LR 704 S - Resomer® LC 703 S ratio 40:60 made by CM.

Table 8
Mechanical parameters calculated from the uniaxial tensile test of blend of Resomer® LR 704 S - Resomer® LC 703 S ratio 40:60 made by CM.

	Young's Modulus [MPa]	Elastic Behaviour Limit[a]	Yielding Stress[b] [MPa]	Yielding Strain[b]	Stress at Failure[b] [MPa]	Strain at Failure[b]
Specimen 1	509.52	0.046	25.31	0.06	31.47	5.89
Specimen 2	528.12	0.049	29.06	0.08	33.40	5.57
Specimen 3	424.49	0.046	22.13	0.06	30.77	6.0
Specimen 4	541.04	0.056	29.47	0.07	15.74	2.78
Specimen 5	503.48	0.061	27.34	0.08	31.85	5.74
Mean ± standard deviation	501.35 ± 45.48	0.051 ± 0.007	26.66 ± 3.02	0.07 ± 0.01	26.51 ± 12.04	5.19 ± 1.36

[a] The elastic behaviour limit defines the maximum engineering strain that can be considered when modelling the material with a linear elastic model.
[b] All the stress and strain are engineering quantities.

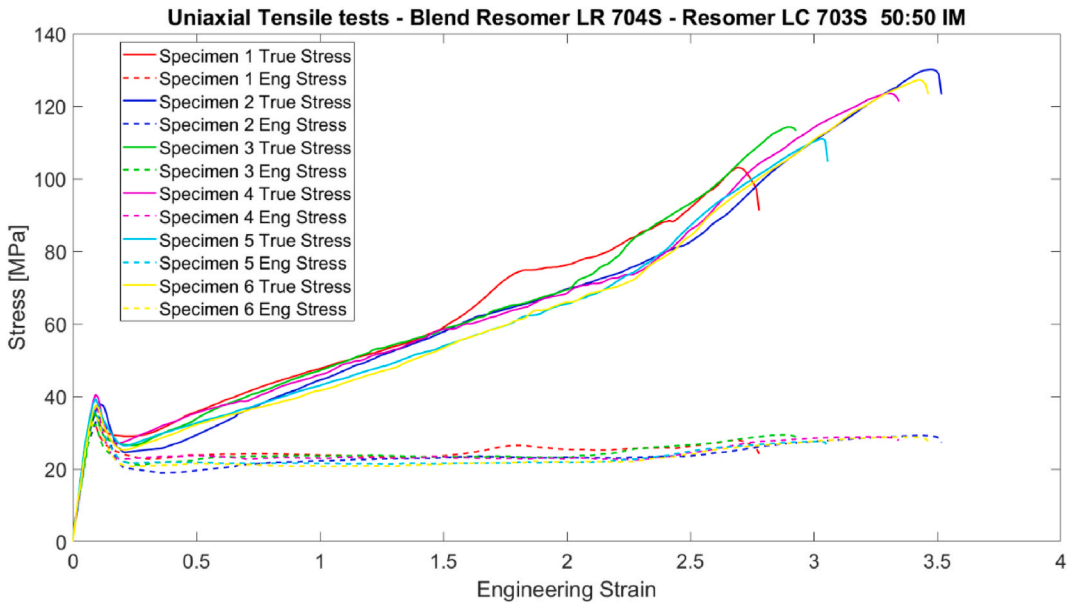


Fig. 8. Uniaxial tensile test results on blend of Resomer® LR 704 S - Resomer® LC 703 S ratio 50:50 made by IM.

3.2.3.1. TNM. The calibration of the TNM on blend specimens with a ratio 50:50 of Resomer® LR 704 S - Resomer® LC 703 S manufactured by CM yielded optimal results. Fig. 13 shows the experimental true stress (continuous) and numerical true stress (dotted). Table 14 reports the TNM constitutive parameters obtained for each specimens evaluated.

3.2.3.2. TNV. Compared to the TNM model, the TNV model also slightly overestimates the strain at which the material yields.

Table 9
Mechanical parameters calculated from the uniaxial tensile test of blend of Resomer® LR 704 S - Resomer® LC 703 S ratio 50:50 made by IM.

	Young's Modulus [MPa]	Elastic Behaviour Limit[a]	Yielding Stress[b] [MPa]	Yielding Strain[b]	Stress at Failure[b] [MPa]	Strain at Failure[b]
Specimen 1	402.69	0.069	33.08	0.08	24.14	2.78
Specimen 2	444.88	0.061	34.40	0.10	27.29	3.52
Specimen 3	389.05	0.080	32.33	0.09	28.83	2.93
Specimen 4	451.11	0.081	37.12	0.09	27.92	3.34
Specimen 5	503.72	0.059	36.02	0.09	25.82	3.06
Specimen 6	482.34	0.061	34.43	0.09	27.61	3.46
Mean ± standard deviation	445.63 ± 44.27	0.069 ± 0.01	34.57 ± 1.78	0.09 ± 0.01	26.94 ± 1.68	3.18 ± 0.30

[a] The elastic behaviour limit defines the maximum engineering strain that can be considered when modelling the material with a linear elastic model.
[b] All the stress and strain are engineering quantities.

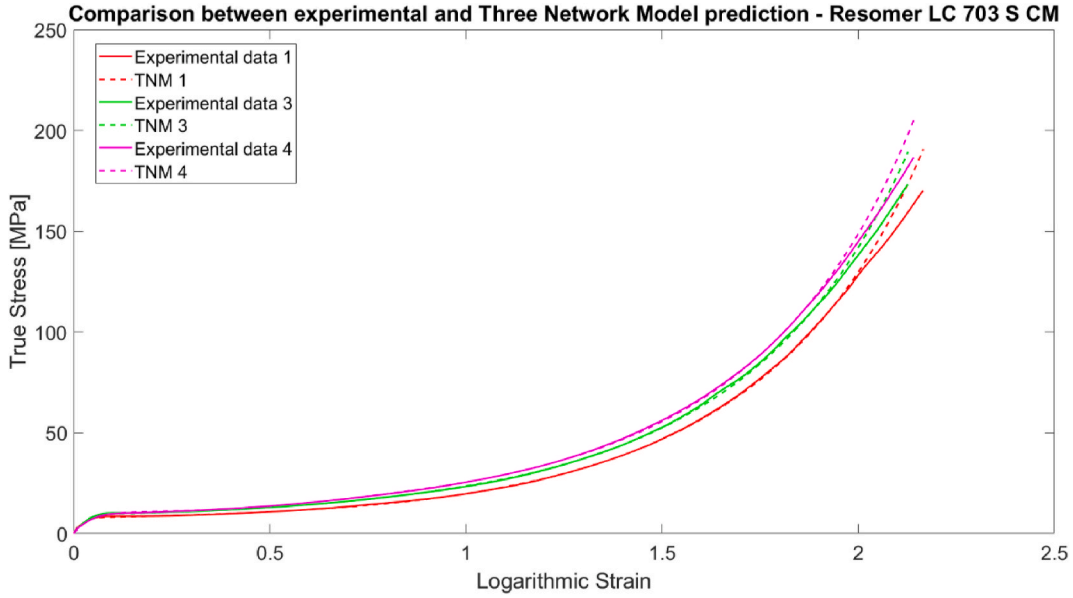


Fig. 9. – Results of the TNM calibration on the experimental data for Resomer® LC 703 S CM.

Table 10
– Material parameters obtained from the calibration of the TNM to capture the behaviour of Resomer® LC 703 S CM. The material parameters controlling the temperature dependence have been omitted since all experiments were performed at room temperature.

	μ_A [MPa]	λ^{lock}	$\hat{\tau}_A$ [MPa]	m_A	μ_{Bi} [MPa]	μ_{Bf} [MPa]	β	$\hat{\tau}_B$ [MPa]	m_B	μ_C [MPa]	R^2
Specimen 1	61.3643	8.8485	15.6802	3.8633	10.0304	0.7605	19.4438	95.6658	5.7034	1.2324	0.9999
Specimen 3	49.9165	9.9911	13.7246	5.4739	10.0342	0.9410	31.7784	99.9601	6.9112	1.2709	0.9998
Specimen 4	52.1901	9.9977	7.6283	19.8969	10.0196	0.3739	91.6558	26.3945	6.9795	1.9308	0.9998

Additionally, the predicted true yielding stress is less accurate as well. Fig. 14 shows the experimental true stress (continuous) and numerical true stress (dotted). Table 15 reports the TNV constitutive parameters obtained for each specimens evaluated.

3.2.4. Constitutive modelling Blend Resomer® LR 704 S - Resomer® LC 703 S ratio 60:40 CM

The following subsections report the results of the numerical calibration of the FEN model to simulate dog-bone blend specimens with a ratio 60:40 of Resomer® LR 704 S - Resomer® LC 703 S manufactured by CM.

3.2.4.1. FEN. The calibration of FEN model on blend specimens with a ratio 40:60 of Resomer® LR 704 S - Resomer® LC 703 S manufactured by CM yielded good results. The model correctly captures the softening behaviour of the biopolymer after yielding. However, the prediction of the yielding point is less accurate. Fig. 15 shows the experimental true stress (continuous) and numerical true stress (dotted). Table 16 reports the FEN constitutive parameters obtained for each specimens evaluated.

3.2.5. Constitutive modelling Blend Resomer® LR 704 S - Resomer® LC 703 S ratio 50:50 IM

The following subsections report the results of the numerical calibration of the two constitutive models under investigation, the TNM and TNV, to simulate dog-bone blend specimens with a ratio 50:50 of Resomer® LR 704 S - Resomer® LC 703 S manufactured by IM.

3.2.5.1. TNM. The TNM calibration on blend specimens with a ratio 50:50 of Resomer® LR 704 S - Resomer® LC 703 S manufactured by IM yielded optimal results. Fig. 16 shows the experimental true stress (continuous) and numerical true stress (dotted). Table 17 reports the TNM constitutive parameters obtained for each specimens evaluated.

3.2.5.2. TNV. Compared to the TNM model, the calibrated TNV model provides less accurate predictions. The estimated yielding point is also less precise. Furthermore, for logarithmic strain values greater than 1, the prediction is overestimated in one case and underestimated in the others. However, in some instances, the overestimation of true stress is

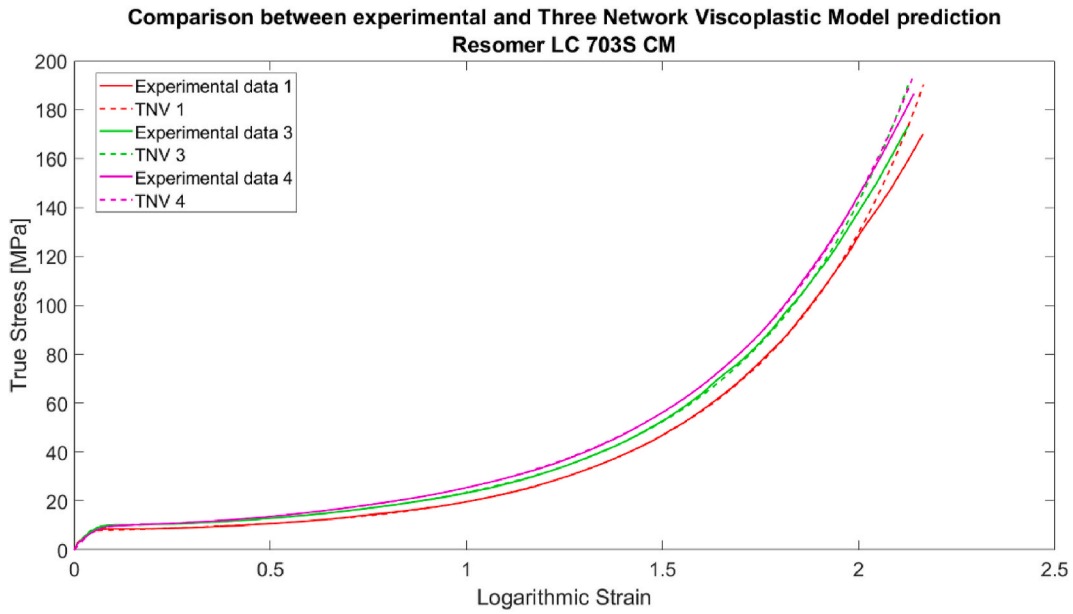


Fig. 10. Results of the TNV calibration on the experimental data for Resomer® LC 703 S CM.

Table 11
Material parameters obtained from the calibration of the TNV to capture the behaviour of Resomer® LC 703 S CM. The material parameters controlling the temperature dependence have been omitted since all experiments were performed at room temperature.

	μ_A [MPa]	λ^{lock}	$\hat{\tau}_A$ [MPa]	m_A	μ_{Bi} [MPa]	μ_{Bf} [MPa]	β	$\hat{\tau}_B$ [MPa]	m_B	μ_C [MPa]	$\hat{\tau}_C$ [MPa]	m_C	R^2
Specimen 1	25.9772	9.9998	6.0143	3.3996	41.6158	0.6096	3.7003	7.1761	6.3837	2.0014	23.2734	18.3591	0.9971
Specimen 3	24.5030	9.9964	5.6392	8.4921	48.6085	4.5077	6.8749	12.4911	3.2298	2.1843	74.3513	6.3660	0.9994
Specimen 4	12.0817	9.9969	4.7331	7.7610	41.8034	4.4272	8.3118	6.6015	7.8217	2.4235	17.0729	2.6565	0.9994

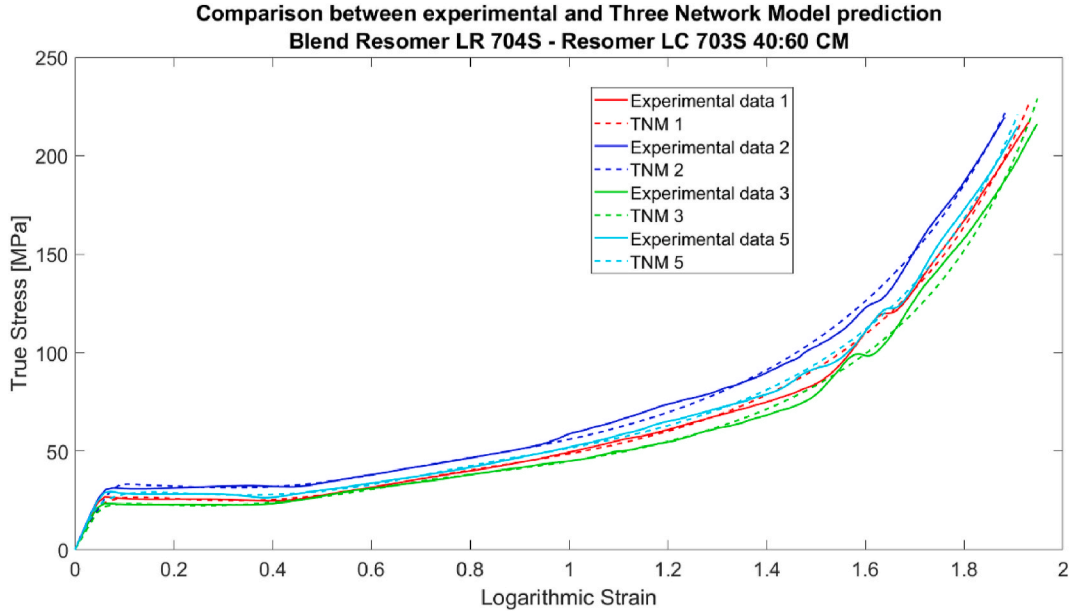


Fig. 11. Results of the TNM calibration on experimental data obtained from blend specimens with a ratio 40:60 of Resomer® LR 704 S- Resomer® LC 703 S CM.

not particularly significant. Fig. 17 shows the experimental true stress (continuous) and numerical true stress (dotted). Table 18 reports the TNV constitutive parameters obtained for each specimens evaluated.

4. Discussion

In this study the TNM, TNV and FEN models were evaluated for the mechanical modelling of commercially available biopolymers and 3 different blends of the manufactured by CM. In particular, Resomer® LR 704 S and LC 703 S and their blend combinations 60:40, 40:60, and

Table 12
Material parameters obtained from the calibration of the TNM to capture the behaviour of blend specimens with a ratio 40:60 of Resomer® LR 704 S- Resomer® LC 703 S CM. The material parameters controlling the temperature dependence have been omitted since all experiments were performed at room temperature.

	μ_A [MPa]	λ^{lock}	$\widehat{\tau}_A$ [MPa]	m_A	μ_{Bi} [MPa]	μ_{Bf} [MPa]	β	$\widehat{\tau}_B$ [MPa]	m_B	μ_C [MPa]	R^2
Specimen 1	72.1127	6.31696	12.7957	6.3495	82.2360	5.0616	9.1846	27.6996	6.05081	3.02105	0.9958
Specimen 2	99.9773	5.2019	21.2343	13.1218	29.0936	2.8240	10.29937	90.9758	2.8243	2.6274	0.9975
Specimen 3	87.9453	5.7683	14.6835	8.1899	50.0971	3.9373	11.7967	19.2782	6.9662	2.5895	0.9937
Specimen 5	83.7723	5.9619	10.2800	12.4786	80.9138	4.8008	8.2102	30.6041	6.1919	2.9018	0.9980

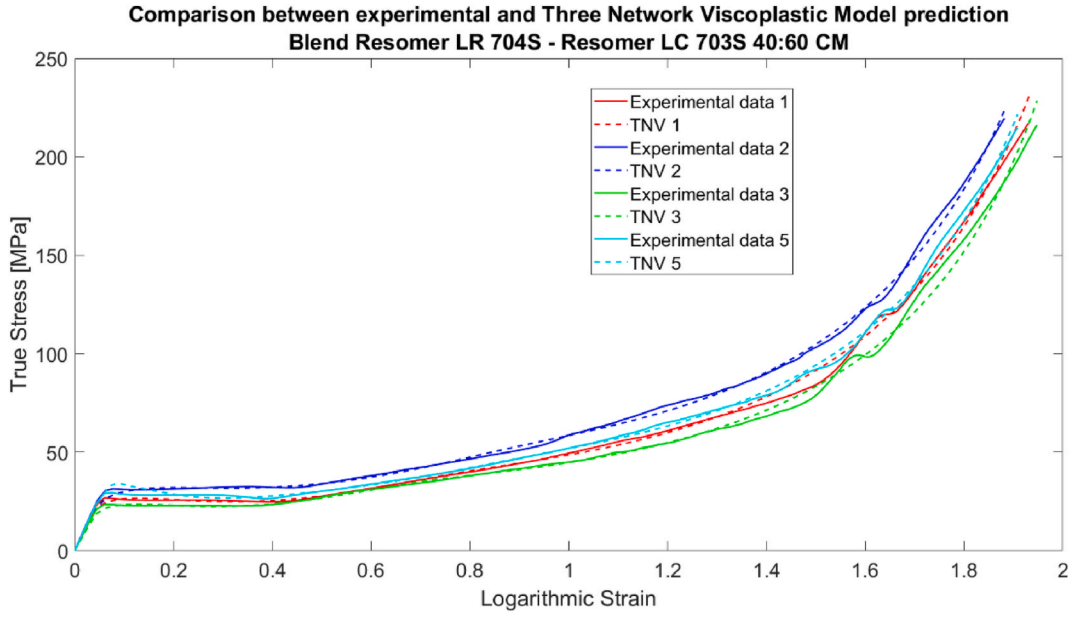


Fig. 12. Results of the TNV calibration on the experimental data obtained from blend specimens with a ratio 40:60 of Resomer® LR 704 S- Resomer® LC 703 S CM.

Table 13
Material parameters obtained from the calibration of the TNV to capture the behaviour of blend specimens with a ratio 40:60 of Resomer® LR 704 S- Resomer® LC 703 S CM. The material parameters controlling the temperature dependence have been omitted since all experiments were performed at room temperature.

	μ_A [MPa]	λ^{lock}	$\widehat{\tau}_A$ [MPa]	m_A	μ_{Bi} [MPa]	μ_{Bf} [MPa]	β	$\widehat{\tau}_B$ [MPa]	m_B	μ_C [MPa]	$\widehat{\tau}_C$ [MPa]	m_C	R^2
Specimen 1	96.5838	6.08472	14.5515	6.3166	80.4374	4.5614	9.5492	25.7047	6.3259	2.9511	99.2066	14.3330	0.9867
Specimen 2	99.7890	6.0673	20.4039	5.8889	62.7238	4.5946	7.5486	40.6191	5.1712	3.1914	98.6167	14.5485	0.9966
Specimen 3	76.1978	5.7858	11.746	7.3044	69.5366	5.1879	10.5187	22.3127	7.40638	2.59858	95.9551	19.3288	0.9892
Specimen 5	78.5634	5.8212	16.4704	19.6456	99.4460	2.4938	17.6072	19.5479	5.9892	2.8011	25.3008	18.7946	0.9958

50:50 (manufactured by CM and IM) were tested. For each biopolymer under investigation more than 4 specimens were tested. Uniaxial tensile tests were conducted to obtain the parameters for the different models.

Considering the biopolymers under investigation, the following results were obtained:

- Specimens of Resomer® LR 704 S manufactured by CM show a linear behaviour. However, since it is a viscoplastic material the mechanical behaviour is influenced by the displacement rate or strain rate. Further experimental tests are needed to evaluate the appropriate constitutive formulation to adopt for FEA. The linear elastic formulation represents a good approximation under the specific condition used. Considering the material as linear elastic we advanced to consider the numerical result reliable for engineering strain below 0,049 ± 0,01.
- Specimens of Resomer® LC 703 S manufactured by CM show the characteristic behaviour of viscoplastic polymers with a yielding point followed by strain hardening behaviour. For this biopolymer the TNM and TNV models were evaluated showing promising results since they were able to capture the mechanical behaviour of the materials with high accuracy. Both models yielded accurate results over the entire deformation range. Based on the calculated R^2 values, the TNM provided a slightly better prediction than the TNV; however, the difference between the two models is minimal. When considering the number of parameters required by each model, the TNM demonstrated a better predictive capability while using only 10 parameters.
- Specimens of the 60-40 blend manufactured by CM exhibit an initial linear elastic behaviour followed by strain softening. Since the FEN model was developed to capture the strain softening behaviour of PLLA, (Dreher et al., 2017) it appears to be the most suitable for representing the mechanical behaviour of this blend. Indeed, the FEN model accurately approximates the mechanical response, demonstrating promising results.
- Specimens of the 50-50 blend manufactured by CM show a linear elastic behaviour initially followed by yielding and strain hardening. The TNM and TNV models were both evaluated for this blend, and both effectively capture its mechanical response. For some specimens, however, neither model was able to accurately reproduce the yielding stress. Overall, the TNM achieved a higher R^2 value for each specimen.

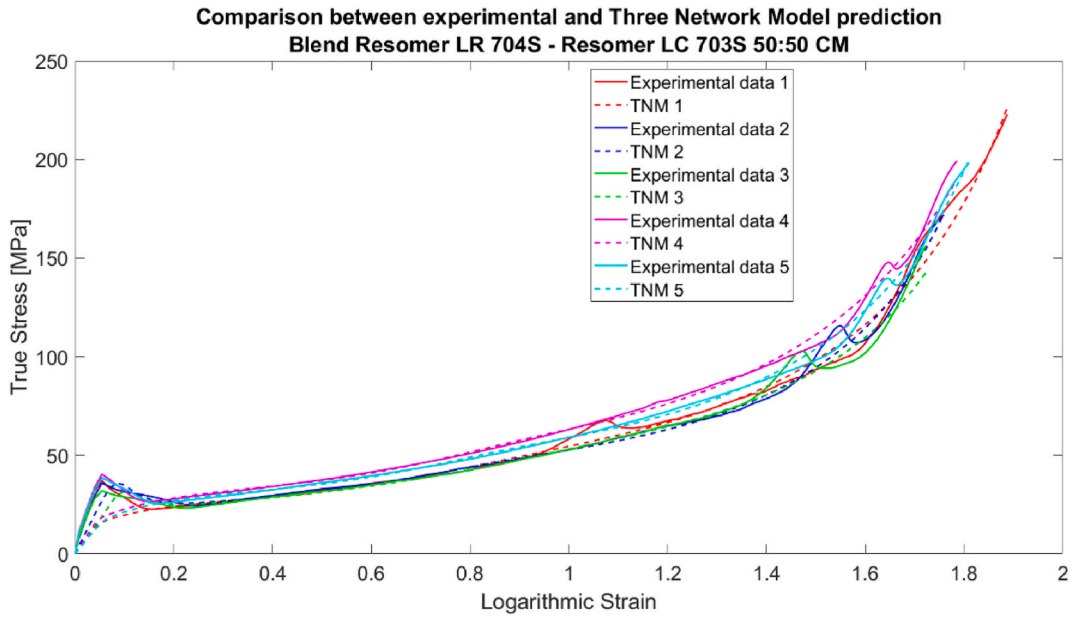


Fig. 13. – Results of the TNM calibration on the experimental data obtained from blend specimens with a ratio 50:50 of Resomer® LR 704 S- Resomer® LC 703 S CM.

Table 14
Material parameters obtained from the calibration of the TNM to capture the behaviour of blend specimens with a ratio 50:50 of Resomer® LR 704 S- Resomer® LC 703 S CM. The material parameters controlling the temperature dependence have been omitted since all experiments were performed at room temperature.

	μ_A [MPa]	λ^{lock}	$\hat{\tau}_A$ [MPa]	m_A	μ_{Bi} [MPa]	μ_{Bf} [MPa]	β	$\hat{\tau}_B$ [MPa]	m_B	μ_C [MPa]	R^2
Specimen 1	76.6219	5.5051	11.9504	6.9041	36.5382	5.6218	5.3772	97.6109	2.9524	2.8721	0.9897
Specimen 2	79.2854	4.5818	22.5328	9.1273	81.3494	3.0685	32.8663	28.5710	4.9050	2.4363	0.9918
Specimen 3	70.3149	4.7941	17.1671	19.7876	40.4198	2.7683	34.7307	86.5309	2.6558	2.2615	0.9808
Specimen 4	82.8233	5.6696	11.7782	9.9271	38.9662	4.9820	4.5983	36.9147	8.4230	3.1470	0.9920
Specimen 5	99.8936	4.8735	19.6386	19.7205	54.8801	2.8906	47.6560	30.7967	5.4677	2.5935	0.9963

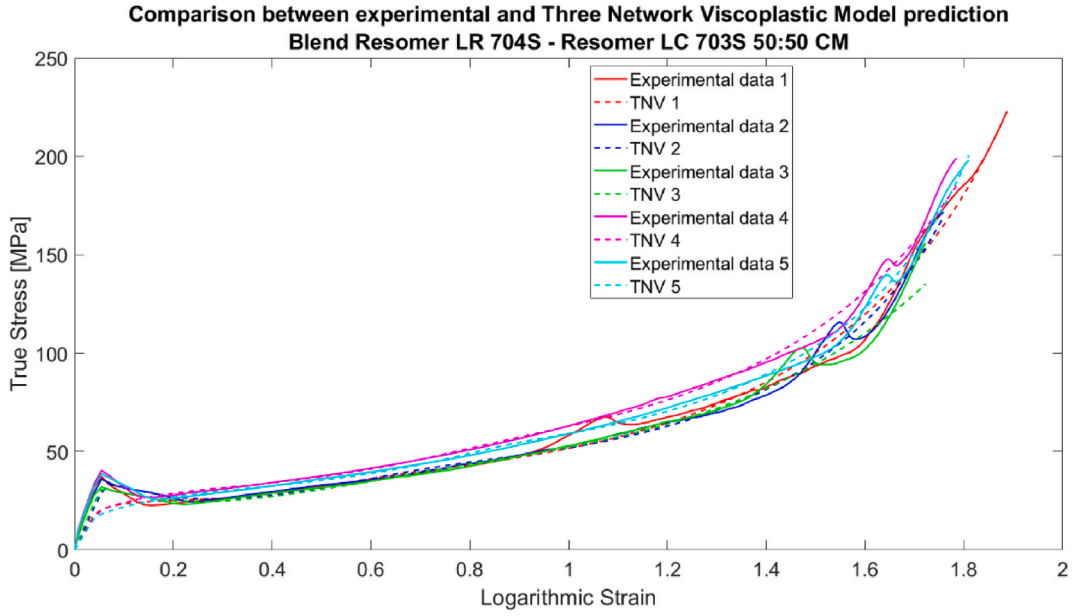


Fig. 14. Results of the TNV calibration on the experimental data obtained from blend specimens with a ratio 50:50 of Resomer® LR 704 S- Resomer® LC 703 S CM.

- Specimens of the 50-50 blend manufactured by IM show similar results to those manufactured by CM, in terms of mechanical behaviour. However, the specimens manufactured by IM show a Young's modulus less than those manufactured by CM. The same results are obtained for the other mechanical parameters calculated. The TNM and TNV models were both evaluated for this blend, and both effectively capture its mechanical response. Based on the calculated

Table 15
Material parameters obtained from the calibration of the TNV to capture the behaviour of blend specimens with a ratio 50:50 of Resomer® LR 704 S- Resomer® LC 703 S CM. The material parameters controlling the temperature dependence have been omitted since all experiments were performed at room temperature.

	μ_A [MPa]	λ^{lock}	$\hat{\tau}_A$ [MPa]	m_A	μ_{Bi} [MPa]	μ_{Bf} [MPa]	β	$\hat{\tau}_B$ [MPa]	m_B	μ_C [MPa]	$\hat{\tau}_C$ [MPa]	m_C	R^2
Specimen 1	99.9481	6.5537	14.4040	7.3355	53.2127	6.3079	9.9491	20.2304	7.4565	3.4633	98.8917	16.2519	0.9018
Specimen 2	75.5548	4.92978	13.5049	14.4463	99.8295	5.5592	15.1251	31.7793	4.9594	2.7215	99.1047	14.6289	0.9740
Specimen 3	99.8365	9.7888	13.5332	19.7491	99.5843	3.9714	17.2992	29.3840	4.2202	3.2315	98.9493	19.1225	0.9877
Specimen 4	99.7755	6.5754	14.1731	10.8254	33.5421	4.7281	5.1199	34.0644	7.1293	3.4339	37.3562	19.1506	0.9063
Specimen 5	15.8080	4.6467	17.4301	19.9189	99.7855	8.8052	33.776	17.4551	7.5494	3.2228	21.0975	4.3665	0.8835

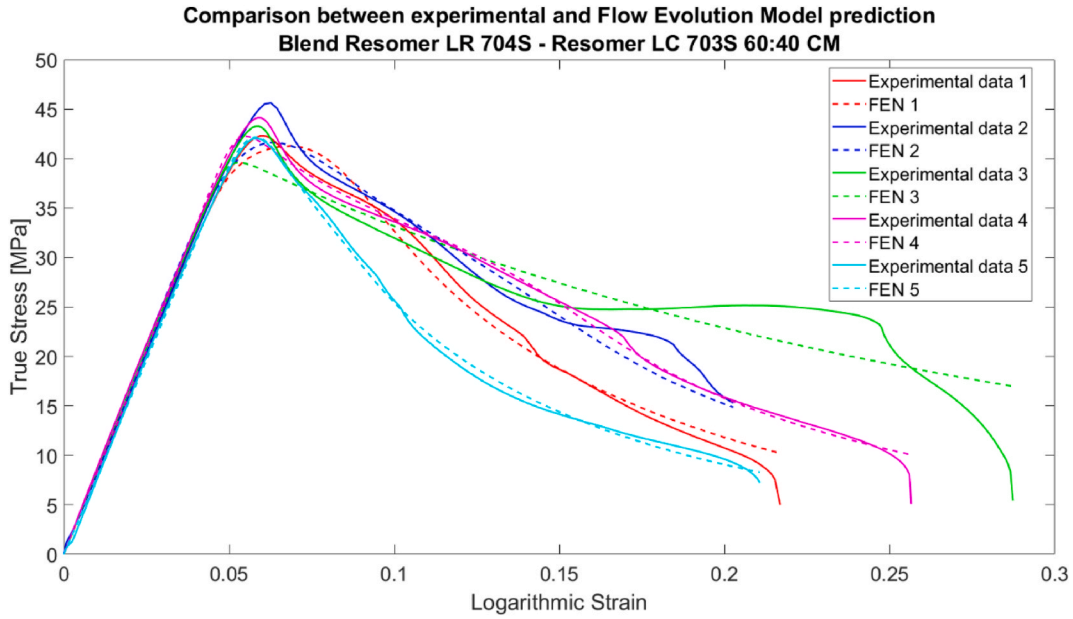


Fig. 15. Results of the FEN model calibration on the experimental data obtained from blend specimens with a ratio 60:40 of Resomer® LR 704 S- Resomer® LC 703 S CM.

Table 16
Material parameters obtained from the calibration of the FEN model to capture the behaviour of blend specimens with a ratio 60:40 of Resomer® LR 704 S- Resomer® LC 703 S CM. The material parameters controlling the temperature dependence have been omitted since all experiments were performed at room temperature.

	C_{10} [MPa]	λ^{lock}	f_B	$\hat{\tau}_A$ [MPa]	m_A	$\hat{\tau}_B$ [MPa]	m_B	g_{SS}	D_e	R^2
Specimen 1	129.2829	8.9667	1.0171	26.6392	12.4078	52.0613	7.1774	0.0077	0.1298	0.9891
Specimen 2	34.2227	8.3321	7.1719	38.0757	3.6339	87.1930	5.2350	0.0542	0.1315	0.9723
Specimen 3	12.8627	8.6622	20.5182	1.5160	6.5930	49.3428	19.1299	0.0747	0.2744	0.9060
Specimen 4	30.2908	8.7400	7.9461	25.9416	5.3653	47.4586	19.3588	0.0058	0.1491	0.9961
Specimen 5	17.3685	9.0081	13.8551	5.5009	18.5681	55.0377	14.2030	0.0400	0.1054	0.9978

R^2 values, the TNM provided a slightly better results compare to the TNV; however, the difference between the two models is minimal.

- Specimens of the 40–60 blend manufactured by CM demonstrate linear elastic behaviour at first, followed by yielding and strain hardening. Both the TNM and TNV models were evaluated for this blend, and each effectively captured its mechanical response. Based on the calculated R^2 values, the TNM provided a slightly better results compare to the TNV; however, the difference between the two models is minimal.

Overall, the calibration results demonstrate that both the TNM and TNV models are suitable for viscoplastic constitutive modelling. Furthermore, they reliably to simulate the mechanical behaviour of biopolymers that show an initial linear elastic behaviour followed by yielding and strain hardening. The procedure used in this study allows accurate calibration of these models. The FEN model demonstrates that it is suitable for simulating the mechanical behaviour of biopolymers blend, correctly predicting the yielding of the biopolymers and showing a good approximation of the strain softening behaviour.

Considering the calculated mechanical parameters (Young's modulus, yield engineering stress and strain, and engineering stress and strain at failure), the following observations can be made:

- Resomer® LR 704 S, manufactured by compression moulding has a mean Young's Modulus of 1040.60 MPa, showing a linear elastic behaviour (see Table 3). However, reducing the displacement rate or strain rate of the tests could show the intrinsic viscoplasticity of the polymer. For this polymer, it was not possible to identify the yielding point, therefore, these two parameters are not reported in Table 4:
- Resomer® LC 703 S, manufactured by compression moulding, exhibits a mean Young's modulus of 121.79 MPa, reflecting the typical behaviour of polymers. Compared with Resomer® LR 704 S, its Young's modulus is approximately one order of magnitude lower, with higher strain at failure but lower stress at failure;
- Blend Resomer® LR 704 S - Resomer® LC 703 S ratio 60:40, manufactured by compression moulding has a mean 746.16 MPa,

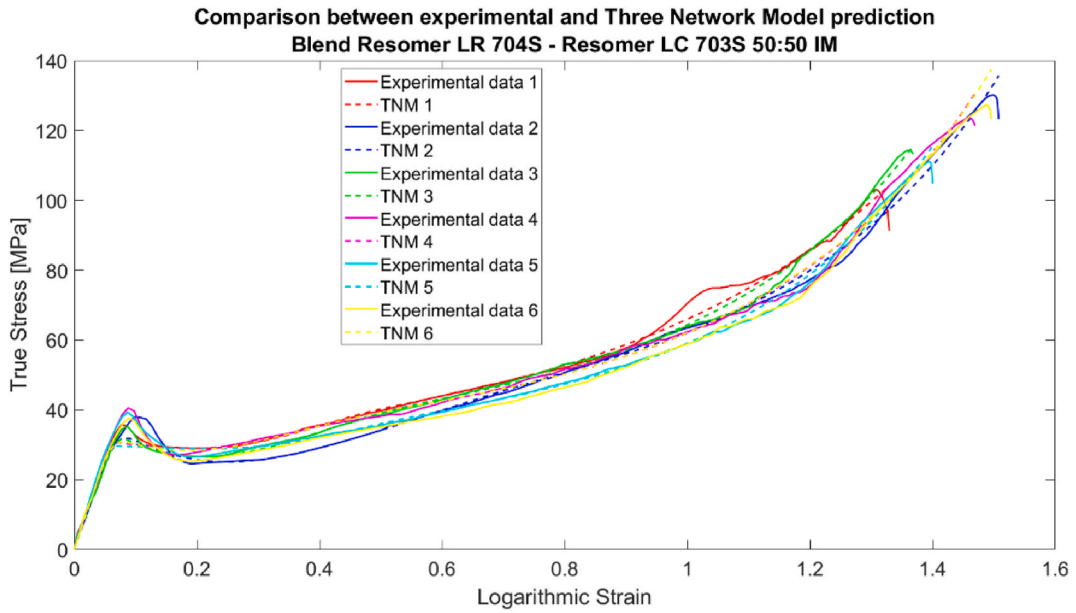


Fig. 16. Results of the TNM calibration obtained from the experimental data on blend specimens with a ratio 50:50 of Resomer® LR 704 S- Resomer® LC 703 S IM.

Table 17
Material parameters obtained from the calibration of the TNM model to capture the behaviour of blend specimens with a ratio 50:50 of Resomer® LR 704 S - Resomer® LC 703 S IM. The material parameters controlling the temperature dependence have been omitted since all experiments were performed at room temperature.

	μ_A [MPa]	λ^{lock}	$\widehat{\tau}_A$ [MPa]	m_A	μ_{Bi} [MPa]	μ_{Bf} [MPa]	β	$\widehat{\tau}_B$ [MPa]	m_B	μ_C [MPa]	R^2
Specimen 1	67.8691	9.0795	13.9897	13.0809	97.5211	9.8414	14.5810	21.5026	8.2716	5.3123	0.9907
Specimen 2	57.4543	4.7705	17.0896	8.0296	99.8200	6.7797	16.6030	89.7390	3.1431	4.2736	0.9956
Specimen 3	61.8887	4.2215	13.8255	15.9911	99.7802	8.6889	19.7331	28.9453	5.8285	4.6883	0.9972
Specimen 4	87.2061	4.6358	14.7590	17.6800	79.1317	9.2554	15.4694	25.8970	5.8809	4.4319	0.9929
Specimen 5	84.8011	3.8466	14.3463	14.1265	98.3008	7.5586	11.3256	22.9496	6.7744	4.0987	0.9956
Specimen 6	74.9497	5.0261	12.1576	13.9582	90.0793	9.7430	14.0873	15.2650	10.4961	4.6772	0.9950

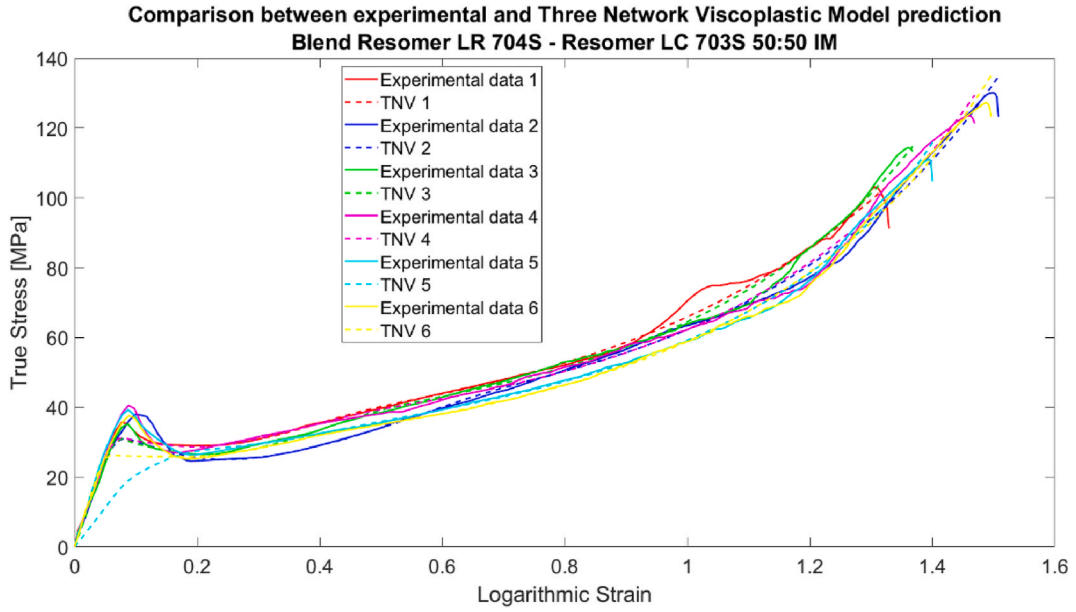


Fig. 17. Results of the TNV calibration obtained from the experimental data on blend specimens with a ratio 50:50 of Resomer® LR 704 S- Resomer® LC 703 S IM.

showing a strain softening behaviour after the yielding strain at 0.06 and yielding stress of 40.96 MPa. The yielding stress of this blend shows a value similar to the failure stress of the Resomer® LR 704 S;

- Blend Resomer® LR 704 S - Resomer® LC 703 S ratio 50:50, manufactured by compression moulding, has a mean Young's modulus of 623.64 MPa. Compared with the 60:40 blend, it shows a decrease in yield stress while maintaining a similar yield strain. Relative to the

Table 18
Material parameters obtained from the calibration of the TNV model to capture the behaviour of blend specimens with a ratio 50:50 of Resomer® LR 704 S - Resomer® LC 703 S IM. The material parameters controlling the temperature dependence have been omitted since all experiments were performed at room temperature.

	μ_A [MPa]	λ^{lock}	$\widehat{\tau}_A$ [MPa]	m_A	μ_{Bi} [MPa]	μ_{Bf} [MPa]	β	$\widehat{\tau}_B$ [MPa]	m_B	μ_C [MPa]	$\widehat{\tau}_C$ [MPa]	m_C	R^2 (100% *of strain*))
Specimen 1	70.6393	9.7644	15.5119	13.2922	95.5068	8.9740	16.0153	19.3969	8.1861	5.3234	94.2831	16.2643	0.9923
Specimen 2	60.6148	5.7149	17.2959	8.8606	95.0547	5.5389	17.4891	24.2651	7.4697	4.6275	98.9345	7.3998	0.9871
Specimen 3	57.4523	4.4738	11.4068	19.6360	96.8731	9.2393	17.5439	23.2338	8.19498	4.7817	97.8348	17.1470	0.9958
Specimen 4	81.7730	4.98741	16.5486	17.6762	99.4536	8.4884	19.6702	21.1382	6.00188	4.5604	99.2205	13.2940	0.9817
Specimen 5	97.4176	3.80532	15.8915	16.9652	83.4019	5.78775	12.5845	21.5959	5.9665	4.0317	37.2471	19.0984	0.9820
Specimen 6	82.2389	5.1177	13.8228	9.2488	97.9269	9.8392	13.5634	14.3853	13.4447	4.7278	27.9522	14.1788	0.9724

original Resomer polymers, this blend exhibits higher yield stress and stress at failure, but lower yield strain and strain at failure compared to Resomer® LC 703 S. In contrast, when compared to Resomer® LR 704 S, it shows reduced stress at failure but increased strain at failure;

- Blend Resomer® LR 704 S - Resomer® LC 703 S ratio 40:60, manufactured by compression moulding, has a mean Young's modulus of 501.35 MPa. Compared with the 50:50 blend, it shows lower yield stress and stress at failure, while yield strain and stress at failure remain comparable. In contrast, compared with the 60:40 blend, it exhibits a decrease in yield stress, an increase in stress and strain at failure, and a comparable yield strain. Relative to Resomer® LC 703 S, this blend shows higher yield stress and stress at failure, but lower yield strain and strain at failure. Finally, compared with Resomer® LR 704 S, it displays a reduction in stress at failure and an increase in strain at failure;
- Blend Resomer® LR 704 S - Resomer® LC 703 S ratio 50:50, "The Resomer® LR 704 S – Resomer® LC 703 S blend (50:50), manufactured by injection moulding, has a mean Young's modulus of 445.65 MPa. Compared with the 40:60 blend, it shows higher yield stress, lower values for the other mechanical parameters, and a comparable stress at failure. Relative to the 60:40 blend, it exhibits a reduction in yield stress but increases in the other parameters. When compared to Resomer® LC 703 S, this blend presents lower strain at failure and higher values for the other parameters. In contrast, compared to Resomer® LR 704 S, it shows an increase in strain at failure and reductions in the other parameters. Finally, relative to the 50:50 blend produced by compression moulding, it shows lower stress and strain at failure, higher yield strain, and a comparable yield stress. Notably, the two manufacturing processes result in specimens with significantly different Young's moduli.

Increasing the amount of Resomer® LR 704 S into the blend formulation lead to an increase in the Young's modulus of the blend reducing the plastic and viscous behaviour. Similar results were reported by Zhao and Zhao (2016) (Zhao and Zhao, 2016), who evaluated the thermal and mechanical properties of different mixtures of commercial PLA (4060D, NatureWorks LLC, Minnetonka, MN, USA) and PCL (CAPA 6500, Perstorp Polyols Inc., Toledo, OH, USA). In particular, they observed that the addition of PCL greatly increased the elongation of the blend, while reducing its tensile strength and modulus (Zhao and Zhao, 2016).

The increase in the percentage of Resomer® LC 703 S in the blend composition leads to a change in the failure behaviour. With higher amounts of Resomer® LC 703 S, the blends exhibit a more ductile failure compared to the brittle behaviour of Resomer® LR 704 S. The increase in PCL content in PLA-PCL blends leads to a transition from brittle to ductile failure (Zhao and Zhao, 2016).

It is important to highlight that the behaviour of these biopolymers presented here is characteristic of the specific deformation speed (0.5 mm/min) used. Since polymers are viscoplastic materials, the loading rate influences the resulting mechanical behaviour (Dreher et al., 2017). Increasing or decreasing the deformation speed alters the response of the polymer. However, further tests are needed to evaluate whether the results of the calibration accurately represent the time-dependent response. The calibration provided in this study for each biopolymer and blend, is able to capture correctly the stress-strain behaviour. However, additional experimental tests are required to validate the obtained calibration, particularly through comparison with stress-relaxation experiments. Stress-relaxation test is essential for correctly calibrate the time-dependent behaviour of polymers and consequently biopolymers. Unfortunately, the amount of biopolymers available were not sufficiently to manufacture more specimens and we were not able to perform experimental stress-relaxation test. Procedure to correctly calibrate materials models for polymers is well documented in the articles reported in the bibliography of this article. Where

sufficient specimens were available for each biopolymer and blend the experimental protocols adopted involve 6 specimens for each test, and at least one stress–strain test at different displacement rates, stress–relaxation tests at various strain levels, and cyclic loading–unloading tests.

5. Conclusion

This study provides new insights into the application of new constitutive laws for viscoplastic materials. The models used in this study, the TNM, TNV and FEN, accurately reproduce the behaviour of commercially available biopolymers. In particular, this work represents one of the first papers where these constitutive models are adopted for biopolymers modelling. The calibration results for these constitutive models reported in the article can support researchers and industries in evaluating the suitability of these biopolymers for developing new medical devices or scaffolds. Overall, the TNM and the TNV models, following the calibration procedure adopted in this study can accurately allow to simulate the mechanical behaviour of these biopolymers. The FEN model, instead, enables prediction of the mechanical behaviour of biopolymers that exhibit strain hardening.

CRediT authorship contribution statement

Vito Burgio: Writing – original draft, Visualization, Methodology, Investigation, Formal analysis, Data curation, Conceptualization. **Martina Di Giacinti:** Writing – original draft, Visualization, Methodology, Investigation, Formal analysis, Data curation. **Mariana Rodriguez Reinoso:** Writing – review & editing, Visualization, Methodology. **Valentina Tuveri:** Writing – review & editing, Visualization, Methodology, Investigation, Formal analysis. **Paola Antonaci:** Writing – review & editing, Visualization, Validation, Methodology. **Cecilia Surace:** Writing – review & editing, Validation, Supervision, Resources, Project administration, Methodology, Funding acquisition.

Declaration of competing interest

The authors declare that they have no known competing financial interests or personal relationships that could have appeared to influence the work reported in this paper.

Acknowledgement

We would like to acknowledge EUREKA! venture SGR spa, to support the project T-REM3DIE (Tendon REpair MEdical DevIcE).

Data availability

Data will be made available on request.

References

Almomani, A., Deveci, S., Mourad, A.H.I., Barsoum, I., 2023. Constitutive model calibration for the thermal viscoelastic-viscoplastic behavior of high density polyethylene under monotonic and cyclic loading. Polym. Test. 118. https://doi.org/10.1016/j.polymertesting.2022.107911.

Anssari-Benam, A., 2024a. Hyperinelasticity: an energy-based constitutive modelling approach to isothermal large inelastic deformation of polymers. Part I. J. Mech. Phys. Solid. 192. https://doi.org/10.1016/j.jmps.2024.105790.

Anssari-Benam, A., 2024b. Hyperinelasticity. Part II: a stretch-based formulation. J. Mech. Phys. Solid. 192. https://doi.org/10.1016/j.jmps.2024.105825.

Anssari-Benam, A., Zaïri, F., 2025. Modelling the finite deformation of thermoplastic polymers via hyperinelasticity. Part I: a semi-crystalline polymer under varying crystallinity ratios and deformation rates. Int. J. Non Lin. Mech. 175. https://doi.org/10.1016/j.ijnonlinmec.2025.105091.

Arruda, E.M., Boyce, M.C., 1992. A THREE-DIMENSIONAL CONSTITUTIVE MODEL FOR THE LARGE STRETCH BEHAVIOR OF RUBBER ELASTIC MATERIALS.

Berardo, A., Polese, L., Carniel, E.L., Toniolo, I., 2024. How does sutures pattern influence stomach motility after endoscopic sleeve gastroplasty? A computational study. Updates Surg. https://doi.org/10.1007/s13304-024-01917-0.

Bergstrom, J.S., 2015. Mechanics of Solid Polymers: Theory and Computational Modeling.

Bergström, J.S., Bischoff, J.E., 2010. An Advanced Thermomechanical Constitutive Model for UHMWPE.

Bergstrom, J., Kurtz, S., Rimnac, C., Edidin, A., 2002. Constitutive modeling of ultra-high molecular weight polyethylene under large-deformation and cyclic loading conditions. Biomaterials 23 (11), 2329–2343. https://doi.org/10.1016/S0142-9612(01)00367-2. ISSN 0142-9612.

Bergstrom, J., Anderson, D., Quinn, D., Schmitt, E., Brown, S., Chow, S., n.d. High Strain Rate Testing and Modeling of Polymers for Impact Simulations.

Bogdanov, B., Vidts, A., Van Den Buicke, A., Verbeeck, R., Schacht, E., 1998. Synthesis and thermal properties of poly(ethylene glycol)-poly(ε-caprolactone) copolymers. Polymer (Guildf.) 39, 1631–1636. https://doi.org/10.1016/S0032-3861(97)00444-8.

Carniel, E.L., Toniolo, I., Fontanella, C.G., 2020. Computational biomechanics: in-silico tools for the investigation of surgical procedures and devices. Bioengineering 7, 1–12. https://doi.org/10.3390/bioengineering7020048.

Diehl, T., Bergstrom, J.S., Liu, X., Lin, L., Zhu, Y., Podhiny, J.J., Chou, R.T., Chambers, J. A., 2013. 2013 SIMULIA Community Conference 1 Combining Detailed Experiments, PolyUMod®, Kornucopia®, and Abaqus® to Create Accurate FE Scratch Simulations.

Dreher, M.L., Nagaraja, S., Bergstrom, J., Hayman, D., 2017. Development of a flow evolution network model for the stress-strain behavior of Poly(L-lactide). J. Biomech. Eng. 139. https://doi.org/10.1115/1.4037071.

Farah, S., Anderson, D.G., Langer, R., 2016. Physical and mechanical properties of PLA, and their functions in widespread applications — a comprehensive review. Adv. Drug Deliv. Rev. 107, 367–392. https://doi.org/10.1016/j.addr.2016.06.012.

Fontanella, C.G., Salmaso, C., Toniolo, I., de Cesare, N., Rubini, A., De Benedictis, G.M., Carniel, E.L., 2019. Computational models for the mechanical investigation of stomach tissues and structure. Ann. Biomed. Eng. 47, 1237–1249. https://doi.org/10.1007/s10439-019-02229-w.

Furmanski, J., 2022. Experimental fracture mechanics analysis of tearing in oriented polyethylene films using digital image correlation and full-field solid mechanics post-processing. Int. J. Fract. 236, 1–31. https://doi.org/10.1007/s10704-021-00600-4.

Guarino, V., Gentile, G., Sorrentino, L., Ambrosio, L., 2017. Polycaprolactone: synthesis, properties, and applications. In: Encyclopedia of Polymer Science and Technology. Wiley, pp. 1–36. https://doi.org/10.1002/0471440264.pst658.

Heiml, E., Kepler, J., 2021. Development of a Design Approach for Individualised 3D-Printed Cellular Polymeric Shoe Soles Eidesstattliche Erklärung.

Holzapfel, G.A., 2002. Nonlinear Solid Mechanics: a Continuum Approach for Engineering Science.

Kumar, S., Singh, S.S., Rozycki, P., 2022. Numerical simulation of strain-softening behavior of glass-filled polymer composites: Comparison of two-dimensional and three-dimensional analyses using Arruda-Boyce and Three-Network viscoplastic models. Mech. Mater. 175. https://doi.org/10.1016/j.mechmat.2022.104481.

Laudon, Matthew, Romanowicz, B.F., 2012. TechConnect summit. Nanotech Conference & Expo 2012 : Nanotechnology 2012 : Technical Proceedings of the 2012 NSTI Nanotechnology Conference and Expo : June 18-21, 2012. Nano Science and Technology Institute, Santa Clara, California, USA.

Li, F., Li, X., He, R., Cheng, J., Ni, Z., Zhao, G., 2020. Preparation and evaluation of poly (D, L-lactic acid)/poly(L-lactide-co-ε-caprolactone) blends for tunable sirolimus release. Colloids Surf. A Physicochem. Eng. Asp. 590, 124518. https://doi.org/10.1016/j.colsurfa.2020.124518.

Pratik, A.R., Powar, R., 2021. Effect of Strain Rate on Continuum and Pre-cracked Polymer Failure Degree Project for Master of Science in Mechanical Engineering-Structural Mechanics.

Quinn, D.J., Bergstrom, J., Chow, S., 2013. Development and experimental validation of an advanced nonlinear. Rate-Dependent Constitutive Model for Polyether Ether Ketone (PEEK).

Reinoso, M.R., Civera, M., Burgio, V., Chiappone, A., Ruiz, O.G., D'anna, A., Riccio, C., Roppolo, I., Frache, A., Antonaci, P., Surace, C., 2021. Effects of the manufacturing methods on the mechanical properties of a medical-grade copolymer poly(L-lactide-co-d,l-lactide) and poly(l-lactide-co-ε-caprolactone) blend. Materials 14. https://doi.org/10.3390/ma14216381.

Stewart, S.A., Domínguez-Robles, J., Donnelly, R.F., Larrañeta, E., 2018. Implantable polymeric drug delivery devices: classification, manufacture, materials, and clinical applications. Polymers 10, 1379. https://doi.org/10.3390/polym10121379.

Teller, S., Bergstrom, J., 2018. 5 Th International LS-DYNA ® Users Conference High Strain Rate Testing and Material Modeling of an Anisotropic Glass Fiber Filled Polyetherimide.

Ugartemendia, J.M., Larrañaga, A., Amestoy, H., Etxeberria, A., Sarasua, J.R., 2018. Tougher biodegradable polylactide system for bone fracture fixations: miscibility study, phase morphology and mechanical properties. Eur. Polym. J. 98, 411–419. https://doi.org/10.1016/j.eurpolymj.2017.11.040.

Zhao, H., Zhao, G., 2016. Mechanical and thermal properties of conventional and microcellular injection molded poly (lactic acid)/poly (ε-caprolactone) blends. J. Mech. Behav. Biomed. Mater. 53, 59–67. https://doi.org/10.1016/j.jmbbm.2015.08.002.